WILEY | Hindawi

Research Article

Development of Nonlinear Geometric Seismic Isolation with a Duffing Spring

Kou Miyamoto [ID],[1] **Jun Iba** [ID],[2] **Koichi Watanabe** [ID],[1] **Ken Ishii** [ID],[3] **and Masaru Kikuchi** [ID][3]

[1]*Institute of Technology, Shimizu Corporation, Tokyo, Japan*
[2]*Graduate School of Engineering, Hokkaido University, Sapporo, Hokkaido, Japan*
[3]*Faculty of Engineering, Hokkaido University, Sapporo, Hokkaido, Japan*

Correspondence should be addressed to Kou Miyamoto; kou.miyamoto16@gmail.com

Seismic isolation is widely used in several countries, and the number of seismically isolated buildings has increased rapidly in recent decades. Seismic isolation extends the natural period of a building to decrease the absolute acceleration and seismic force. As there is a trade-off between the absolute acceleration and displacement, a soft layer results in a large displacement for a large seismic wave, but the hard one causes the large absolute acceleration even for a small seismic wave. The restoring force of a Duffing spring is given by the third and first orders of the displacement. This spring has been applied to protect a building from large earthquake waves. However, the influence of the coefficient of the Duffing spring that determines the dynamic characteristics of the system has not been clarified. Thus, a used Duffing spring may not be appropriate for seismic resistance. Moreover, most studies are based on analytical methods, and the advantages of the Duffing isolation have not been verified in an actual system. To address these problems, this paper reveals the influence of the coefficient of the Duffing spring on structural responses to seismic waves. Moreover, this paper devised a way to implement a Duffing spring for seismic isolation and carried out experiments to verify the validity in actual systems. The experimental results presented that the Duffing spring was effective in protecting a building in actual systems.

1. Introduction

Passive isolation has been applied in several fields [1]. In civil engineering, seismic isolation has been used to protect buildings from large earthquakes. To date, several buildings have employed seismic isolation. In Japan, the number of seismically isolated buildings has increased rapidly after the Great Hanshin earthquake (Kobe earthquake) [2].

Seismic isolation introduces a soft layer into a building to extend its natural period to suppress the absolute acceleration. However, as there is a trade-off between the displacement and absolute acceleration, the displacement of a seismically isolated layer might exceed an allowable range. To overcome this disadvantage, nonlinear devices are used and invented such as lead dampers, steel dampers, and high-damping rubber bearings [3]. In recent times, new seismic-isolation devices have been developed, for example,

nonlinear geometric isolation [4], isolation with an inerter [5, 6], dual-mode isolation, which has a bilinear spring [7], and triple friction pendulum bearings [8].

On the other hand, the restoring force of the Duffing spring is given by the third and first orders of the displacement, which has been applied to isolation systems, e.g., [9–17]. The dynamic behavior of the Duffing oscillator that has both a Duffing spring and a linear spring is complicated because of the occurrence of the jump phenomenon, which causes bifurcation [9]. Several studies have estimated the performance of the Duffing oscillator.

Tamas et al. considered a forced and free response of the Duffing oscillator and compared its dynamic behavior and that of a linear system [9]. While a linear single-degree-of-freedom (SDOF) system possesses one resonance frequency, the Duffing oscillator with weak damping exhibits a secondary resonance frequency, which is subharmonic

resonance. Carrella et al. defined a simple equation that estimates the peak gain of transmissibility of an external force to displacement [10]. The peak transmissibility of a linear system depends on a damping ratio. In contrast, the transmissibility of the Duffing oscillator depends not only on the damping ratio but also on the coefficient of the Duffing spring and the maximum steady-state response.

Recently, the Duffing spring has been applied to vibration isolation in mechanical engineering. The Duffing spring can be achieved using multiple springs [10], electrical devices [11], or magnets [12]. The advantages of using electronic or magnetronic devices are long strokes and long life spans. Zhang et al. presented a torsion-translational vibration isolator based on convex ball-roller mechanisms that isolate torsion and translational vibration [13]. Wang et al. presented a dual quasi-zero stiffness-based vibration isolator that uses additional springs to improve the control performance of the Duffing oscillator [14].

The stiffness of the Duffing spring is given by the square of the displacement; the stiffness of the Duffing spring is small for small displacements and becomes large for a significant displacement. Thus, the Duffing spring compensates for the drawback of seismic isolation. That is, the combination of seismic isolation and the Duffing spring suppresses the absolute acceleration for a small displacement and suppresses the displacement for a large earthquake. The Duffing spring has been applied for seismic isolation to protect a building (Duffing isolation). Watanabe and Nakai showed that Duffing isolation with an inerter was effective in reducing the displacement and absolute acceleration [15]. Zhou et al. used the Duffing spring to suppress the vertical vibration of a building and showed that the Duffing spring is effective in reducing transmissibility [16]. Liu et al. analyzed the control performance of Duffing isolation for near-fault ground motion and demonstrated that Duffing isolation exhibits good control performance with regard to the displacement of earthquake waves [17]. These studies demonstrated that the combination of Duffing isolation yields adequate control performance. Although the dynamic characteristic of Duffing isolation is determined by the coefficient of the Duffing spring, the influence of the coefficient of the Duffing spring on the structural responses remains unclear. Furthermore, these studies are based on analytical ways, and the advantage has not been verified in an actual system. To address these problems, this paper reveals the influence of the Duffing spring on the structural response to seismic waves. Moreover, to verify the advantage of Duffing isolation in actual systems, this paper devised a way to implement a Duffing spring in seismic isolation and carried out an experiment in a full-scale displacement model. The experimental results demonstrated that Duffing isolation is effective in protecting a building from seismic waves in an actual system.

This paper is organized as follows: Section 2 explains the dynamic characteristics of the Duffing oscillator and shows the difference from a linear system. Section 3 investigates the control performance and the dynamic characteristic of seismic isolation with the Duffing spring with time history analysis (THA). The THA results present that the absolute acceleration of Duffing isolation is at the same level with an ordinary seismic isolation model for small waves. In contrast, Duffing isolation suppresses the maximum displacement for large waves. Furthermore, this paper presents a way to adjust the coefficient of the Duffing spring. Section 4 implements and explains the use of a Duffing spring device for seismic isolation. Unlike other studies, this study devises a way to implement a Duffing spring for a seismic isolation model and shows that Duffing isolation is effective in suppressing the responses in actual equipment. Moreover, this section shows that the THA closely agrees with the experimental results. Section 5 concludes the paper.

2. Fundamental Characteristics of the Duffing Oscillator

This section explains the equation of motion and derives the steady-state response of the Duffing oscillator to explain its dynamic characteristics based on Carrella's results [10]. In this paper, the restoring force of a Duffing spring, $F_n(x(t))$ [N], is given by the following equation:

$$
\begin{aligned}
F_n(x(t)) &= \Lambda_{N1} x(t) + \Lambda_{N3} x^3(t) \\
&= [k_{N1} + k_{N3}(x(t))] x(t),
\end{aligned}
\tag{1}
$$

where $x(t)$ [m] is the displacement, Λ_{N1} [N/m] and Λ_{N3} [N/m^3] are the coefficients of the Duffing spring, and k_{N1} [N/m] and $k_{N3}(x(t))$ [N/m] are the stiffness of the Duffing spring.

The Duffing spring can be achieved using two orthogonal springs (Figure 1(a)), and the dynamics of the Duffing oscillator is as follows:

$$
m\ddot{x}(t) + c\dot{x}(t) + kx(t) + F_n(x(t)) = -m\ddot{x}_g(t),
\tag{2}
$$

where m [kg] is the mass, c [N · s/m] is the damping coefficient, k [N/m] is the stiffness, $F_n(x(t))$ is the restoring force of the Duffing spring, and $\ddot{x}_g(t)$ [m/s^2] is the ground acceleration. The restoring force of the two orthogonal springs, $F_n(x(t))$, can be approximated by the third Taylor polynomial of the function [10], and the coefficients, namely, k_{N1}, k_{N3}, Λ_{N1}, and Λ_{N3}, are given as follows:

$$
\left\{
\begin{array}{ll}
\Lambda_{N1} = 2k_{ort}\left(1 - \dfrac{d_0}{d}\right), & \Lambda_{N3} = k_{ort}\dfrac{d_0}{d^3}, \\[2ex]
k_{N1} = \Lambda_{N1}, & k_{N3}(x(t)) = \Lambda_{N3} x^2(t).
\end{array}
\right.
\tag{3}
$$

In the equation, k_{ort} [N/m] is the stiffness of the orthogonal spring, d_0 [m] is the natural length of the orthogonal spring, and d [m] is the set length of the orthogonal spring. Hence, the Duffing oscillator is explained in Figure 1(b). It is worth mentioning that if orthogonal springs are compressed at the equilibrium position, then the restoring force of the Duffing spring, $F_n(x(t))$, takes a negative
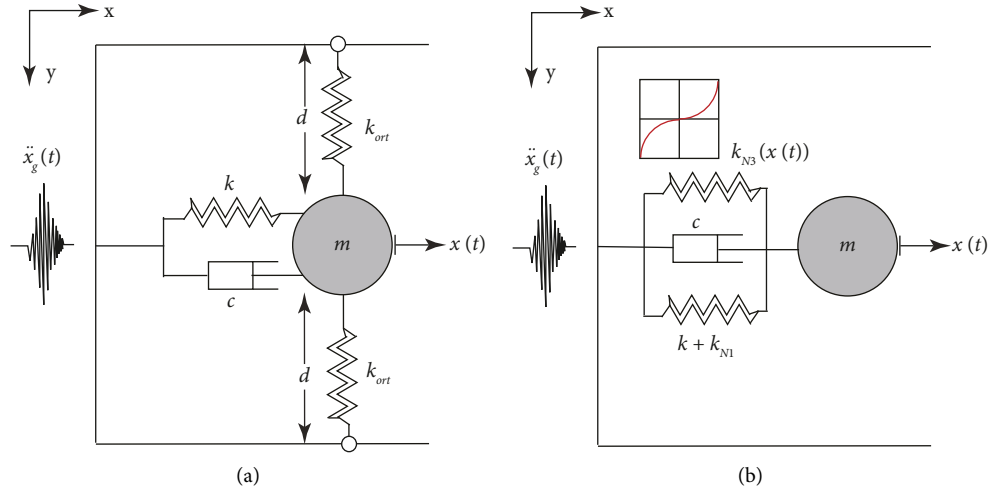
FIGURE 1: Duffing isolation models: (a) original model and (b) equivalent model.

value for small displacements because $d_0 > d$, and it results that Λ_{N1} is a negative value [18]. In other words, negative stiffness can be achieved for a small displacement. In contrast, this study used unstretched springs, that is, $d = d_0$ and $\Lambda_{N1} = 0$. Thus, $F_n(x(t))$ can be approximated by

$$F_n(x(t)) = \Lambda_{N3} x^3(t)$$
$$= k_{ort} \frac{1}{d_0^2} x^3(t). \tag{4}$$

Equation (4) shows that the restoring force of the Duffing spring is yielded based on the cube of the displacement. In other words, the stiffness depends on the displacement and is given by the square of the displacement. Namely, the stiffness of the Duffing spring, $k_{N3}(x(t))$, is small for small displacements and large for large displacements. This point is one of the big differences in linear stiffness. Derivations of equations (1) and (3) are explained in Appendix A.

Rewriting equation (2) yields the following equation:

$$\ddot{x}(t) + 2\xi\omega_s\dot{x}(t) + \omega_s^2 x(t) + \lambda_s x^3(t) = -\ddot{x}_g(t), \tag{5}$$

where

$$\xi = \frac{c}{2m\omega_s},$$

$$\omega_s = \sqrt{\frac{k}{m}}, \tag{6}$$

$$\lambda_s = \frac{\Lambda_{N3}}{m}.$$

In the equation, ξ indicates the damping ratio for the natural circular frequency, ω_s (rad/s).

To consider the steady-state response of the system, this paper assumes that the ground motion $\ddot{x}_g(t) = -a_e \cos\Omega t$, where a_e (m/s²) is the amplitude and Ω (rad/s) is the circular frequency of the wave. This paper assumes that the response of system equation (2) can be approximated as

$$x(t) = r\cos(\Omega t + \phi), \tag{7}$$

where ϕ (rad) is the phase of the wave and r (m) is the amplitude. As shown in previous studies such as [19], the amplitude, r, is given by

$$r = \pm \frac{a_e}{D(\Omega)}, \tag{8}$$

where

$$D(\Omega) = \sqrt{(2\xi\omega_s\Omega)^2 + \left(\omega_s^2 + \frac{3}{4}\lambda_s r^2 - \Omega^2\right)^2}. \tag{9}$$

Suppose that the damping ratio is much smaller than 1, $\xi \ll 1$, then equation (8) takes the peak value, i.e., r_p, if Ω satisfies $\omega_s^2 + 3/4\lambda_s r^2 - \Omega^2 = 0$. In this case, Ω is defined as a resonance circular frequency, Ω_p (rad/s):

$$\Omega_p = \sqrt{\omega_s^2 + \frac{3}{4}\lambda_s r_p^2}. \tag{10}$$

The resonance circular frequency of an undamped linear system, $\Omega_{p,\mathrm{lin}}$, is given as follows:

$$\Omega_{p,\mathrm{lin}} = \omega_s, \tag{11}$$

$\Omega_{p,\mathrm{lin}}$ is the same as equation (10) with $\lambda_s = 0$. Since $k_{N3}(x(t))$ is a function of the displacement, equation (10) reflects its characteristic.

The peak amplitude for a sinusoidal wave, r_p, is given by the following equation (12):

$$r_p = \pm \sqrt{\frac{2}{3\lambda_s}\left(\sqrt{\omega_s^4 + \frac{3\lambda_s}{4\xi^2\omega_s^2}a_e^2} - \omega_s^2\right)}. \tag{12}$$

3. Seismic Response and Influence of the Duffing Spring

This section shows the seismic response of Duffing isolation, which has both a Duffing spring and a soft linear spring, and clarifies the influence of the Duffing spring coefficient on the structural responses. This paper adjusts the coefficient of the Duffing spring, Λ_{N3}, in a manner such that the restoring force of the Duffing spring, $\Lambda_{N3}x^3(t)$, is the same as that of the linear spring, $kx(t)$, at the selected displacement, x_{sel} (m):

$$\Lambda_{N3} = k\frac{1}{x_{\text{sel}}^2}. \tag{13}$$

The stiffness of the whole system, k_{all} (N/m), is given by

$$k_{\text{all}}(x(t)) = k + \Lambda_{N3}x^2(t). \tag{14}$$

Substituting equation (13) and $x(t) = x_{\text{sel}}$ into equation (14) gives that

$$k_{\text{all}}(x_{\text{sel}}) = k + k\frac{1}{x_{\text{sel}}^2}x_{\text{sel}}^2 = 2k. \tag{15}$$

That is, the stiffness of the whole system is twice as k when the displacement is x_{sel}. Note that $\Lambda_{N3}x^2(t)$ might be small for $x(t) < x_{\text{sel}}$. This study models a seismic-isolated structure as an SDOF model, and the linear stiffness of the isolation system, k, is given by

$$k = \frac{4\pi^2}{T_s^2}m, \tag{16}$$

where T_s(s) is a natural period of the model.

The parameters of the models, namely, mass (m) is 4038 kg; natural periods (T_s) are 1.0 s, 2.0 s, 3.0 s, and 4.0 s; the damping ratios (ξ) are 0.01, 0.04, 0.07, 0.1, and 0.15; the selected displacements for the Duffing springs (x_{sel}) are 0.1 m, 0.3 m, 0.6 m, and 0.01 m ~ 0.8 m; and the clearance, which is an allowable displacement range (x_{cle}), is 0.65 m. Note that mass is decided by the specimen used in Section 4. The damping ratio of seismic isolation is around 0.10 ~ 0.20. Thus, $\xi = 0.10$ and 0.15 indicate the standard damping ratios of seismic isolation. To clarify the characteristics of the Duffing spring, this paper uses some smaller damping ratios ($\xi = 0.07$, 0.04, and 0.01).

In general, the natural period of a seismic isolation system is longer than 2.0 s in Japan [3]. However, to make the characteristics of Duffing isolation clear, this section uses the model that assumes the natural period as 1.0 s.

This section uses five models in which two are linear models and the other three are Duffing isolation models as follows:

  (i) [1] Soft model (S model): a linear model with linear stiffness is given by equation (16)
  (ii) [2] Hard model (H model): a linear model with stiffness is given by equation (17):

$$k_H = k + k\frac{1}{0.3^2}0.65^2. \tag{17}$$

  (iii) [3–5] Duffing isolation models that x_{sel} are 0.1 m, 0.3 m, and 0.6 m; respectively.

In equation (17), $k/0.3^2$ is the coefficient of the Duffing spring with $x_{\text{sel}} = 0.3$ m and k_H is identical to the stiffness of Duffing isolation with a displacement of 0.65 m. The S, H, and Duffing isolation models with $x_{\text{sel}} = 0.3$ m indicate the models with soft linear stiffness, hard linear stiffness, and the nonlinear stiffness that vary from soft to hard, respectively. The stiffness of the Duffing isolation depends on the displacement. For example, the stiffness of the $x_{\text{sel}} = 0.3$ m model, $k + k/0.3^2$, varies in $k \leq k + k/0.3^2 \leq k_H$ for $x < x_{\text{cle}}$. The comparison of Duffing isolation with the S and H models makes the difference between the Duffing isolation model with $x_{\text{sel}} = 0.3$ m models and linear systems clear. This section uses 44 recorded waves and one artificial wave (random wave) (Figure 2). The 44 waves are recommended to evaluate the vibration-suppression performance by the Federal Emergency Management Agency (FEMA) P695 [21]. The accelerogram and the pseudo velocity spectrum, $_pS_V$, of the random wave are shown in Figure 2.

Note that this paper assumes that the absolute acceleration of Duffing isolation takes a maximum value when the displacement is maximum, x_{max}. The equation estimating the maximum absolute acceleration of Duffing isolation is given as follows:

$$\left|\ddot{x} + \ddot{x}_g\right|_{\text{max}} \approx \frac{1}{m}\left(kx_{\text{max}} + \Lambda_{N3}x_{\text{max}}^3\right). \tag{18}$$

Figure 3 shows the THA results of the S and H models and the three Duffing isolation models ($x_{\text{sel}} = 0.1$ m, $x_{\text{sel}} = 0.3$ m, and $x_{\text{sel}} = 0.6$ m). The results show that the relationship between the maximum displacement and absolute acceleration is linear for the S and H models. In contrast, the relationship between the three Duffing isolation models is not linear because their stiffness is a function of the displacement. The comparison of the S and Duffing isolation models shows that the maximum absolute acceleration of both of them is almost the same for a small displacement.

To compare the maximum absolute acceleration of an H model and a Duffing isolation model, the following equation is used to estimate the maximum acceleration of the H model:

$$\left|\ddot{x} + \ddot{x}_g\right|_{\text{max},Hmdl} = \frac{k_H}{m}x_{\text{max}}. \tag{19}$$

This equation is based on the relationship between the displacement and the acceleration response spectra. Substituting (17) into (19) yields

$$\left|\ddot{x} + \ddot{x}_g\right|_{\text{max},Hmdl} \approx \frac{k}{m}x_{\text{max}}\left(1 + \frac{0.65^2}{0.3^2}\right) = \omega_s^2 x_{\text{max}}\left(1 + \frac{0.65^2}{0.3^2}\right). \tag{20}$$
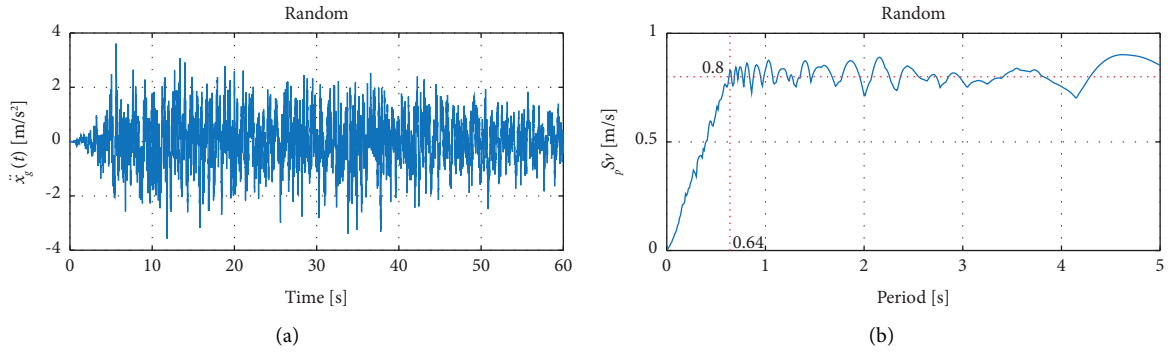
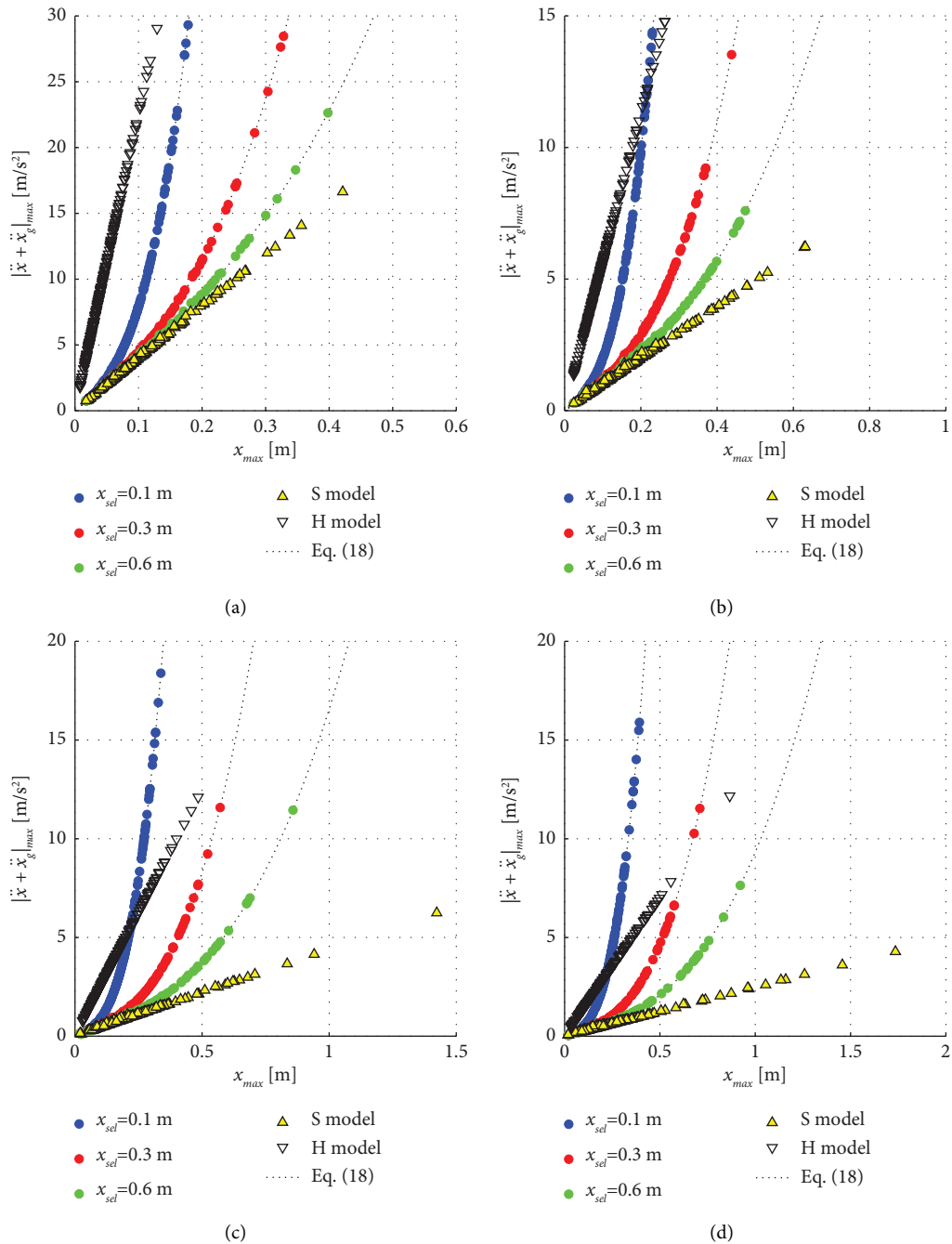FIGURE 2: Random wave: (a) accelerogram and (b) pseudo velocity spectrum ($\xi = 5\%$).

FIGURE 3: Comparison between Duffing isolation and linear systems with equation (18) for several T_s [s]: (a) $T_s = 1.0$ s, (b) $T_s = 2.0$ s, (c) $T_s = 3.0$ s, and (d) $T_s = 4.0$ s with the damping ratios $\xi = 0.01, 0.04, 0.07, 0.1,$ and 0.15 for 44 waves.

On the other hand, the maximum acceleration of the Duffing isolation model ($x_{sel} = 0.1$ m) is given by equation (18). That is, equations (13) and (18) give

$$\left|\ddot{x} + \ddot{x}_g\right|_{\max} \approx \frac{1}{m}\left(kx_{\max} + k\frac{1}{x_{sel}^2}x_{\max}^3\right) = \omega_s^2 x_{\max}\left(1 + \frac{x_{\max}^2}{x_{sel}^2}\right). \tag{21}$$

The maximum displacement, $\tilde{x}_{\max}$, such that the maximum absolute acceleration of the H model and the Duffing isolation model is the same, is given by substituting equations (21) into (19):

$$\tilde{x}_{\max} = \frac{0.65}{0.3}x_{sel} \approx 2.17x_{sel}. \tag{22}$$

For example, the absolute acceleration of the H and Duffing isolation models with $x_{sel} = 0.1$ m is at the same level if their maximum displacements are approximately 0.22 m.

Figure 4 shows the maximum displacement and absolute acceleration of the Duffing isolation models. This figure shows the relationship between x_{sel} and the responses for several damping ratios, ξ, and earthquake waves. In this figure, the Kobe (NIS000), Chi-Chi (CHY101-E), and random waves are used. The results show that there is a trade-off between the maximum displacement and absolute acceleration. A small x_{sel} value results in small displacements and large absolute acceleration, and vice versa. The maximum displacement, $x_{\max}$, converges to a value as x_{sel} increases. The coefficient of the Duffing spring Λ_{N3} decreases as x_{sel} increases. Hence, the behavior of the Duffing isolation model with high x_{sel} is closely similar to that of the S model. Owing to this reason, Figure 4 shows that the maximum displacement converges as x_{sel} increases.

The Duffing spring with small x_{sel} causes the large absolute acceleration but suppresses the maximum displacement for seismic waves. In contrast, large x_{sel} may be beyond the clearance, but the maximum absolute acceleration is at the same level as that of the S model, which is the seismic isolation model. This result reflects equation (18) (Figure 3).

Next, the influence of the amplitude of the input wave on the control performance of Duffing isolation is assessed. This paper uses the random wave with a scaling factor γ. The input wave is given by $\gamma \ddot{x}_g(t)$. As an example, this paper uses the model with the natural period, T_s, and damping ratio, ξ, as 3.0 s and 0.04, respectively. Figure 5 shows the relationship between γ and the maximum displacement (Figure 5(a)), the absolute acceleration of the model (Figures 5(b) and 5(c)), and the restoring force (Figure 5(d)). Figure 6 shows the THA results of the displacement and absolute acceleration for $\gamma = 0.5, 1.0, 1.5,$ and 2.0.

Figure 5(d) shows that the maximum restoring force of the Duffing isolation models is almost at the same level as that of the S model for small values of γ. In contrast, if the value of γ becomes large, the maximum restoring force of the Duffing isolation model is bigger than that of the S model. Figures 5 and 6 show that the maximum displacements and absolute acceleration of the Duffing isolation models are at the same level as those of the S model for small γ. On the other hand, if the value of γ becomes large, the maximum displacements of the Duffing isolation models are smaller than those of the S model. In particular, the maximum displacement of the Duffing isolation model with $x_{sel} = 0.1$ m is almost the same as that of the H model. Figure 7 shows the displacement and the sum of the restoring force of the Duffing spring and the linear spring $F_{Res}(t)$ (N), i.e.,

$$\begin{aligned} F_{Res}(t) &= \Lambda_{N3}x^3(t) + kx(t) \\ &= [k_{N3}(x(t)) + k]x(t). \end{aligned} \tag{23}$$

Figure 7 demonstrates the characteristic of Duffing isolation. Although the relationship between the restoring force and displacement is almost linear for small waves ($\gamma = 0.5$) with large x_{sel} values, the restoring force increases sharply if the displacement becomes large such as the case of $\gamma = 2.0$, especially for the model with small x_{sel}. This is one of the biggest differences between Duffing isolation (Duffing oscillators) and linear systems. $k_{N3}(x(t))$ is large for large displacements and suppresses the displacement, but stiffness is small for small displacements.

The design process of Duffing isolation is as follows:

Step 1: the earthquake waves used for the design are selected

Step 2: the linear stiffness, k, and the damping ratio, ξ, of seismic isolation are designed

Step 3: the value of x_{sel} is chosen so that responses could satisfy the requirement

Step 4: If any x_{sel} values do not meet the requirement, then the damping ratio of seismic isolation is increased

Step 5: If the result still does not meet the criteria, then the linear stiffness of the seismic isolation, k, is adjusted

This section assesses the control performance of Duffing isolation for seismic waves and clarifies the influence of the Duffing spring coefficient on structural responses. One of the biggest differences between Duffing isolation and the linear system is that the stiffness of the Duffing spring depends on the displacement. That is, the stiffness of the whole system is low for small displacements, and the maximum absolute acceleration is at the same level as that of the linear model with a soft spring (S model). In contrast, if the amplitude of the input wave becomes large, the Duffing spring reduces the displacement. Hence, the combination of seismic isolation and the Duffing spring is effective in reducing the displacement for large seismic waves and suppressing the absolute acceleration for small waves.

The next section implements the Duffing spring for seismic isolation and verifies the validity of Duffing isolation.

4. Experiment for Duffing Isolation

This section shows the experimental setup and results. The experiment was carried out at Institute of Technology of Shimizu Corporation. This paper developed Duffing isolation and S models and compared their responses for several seismic waves.
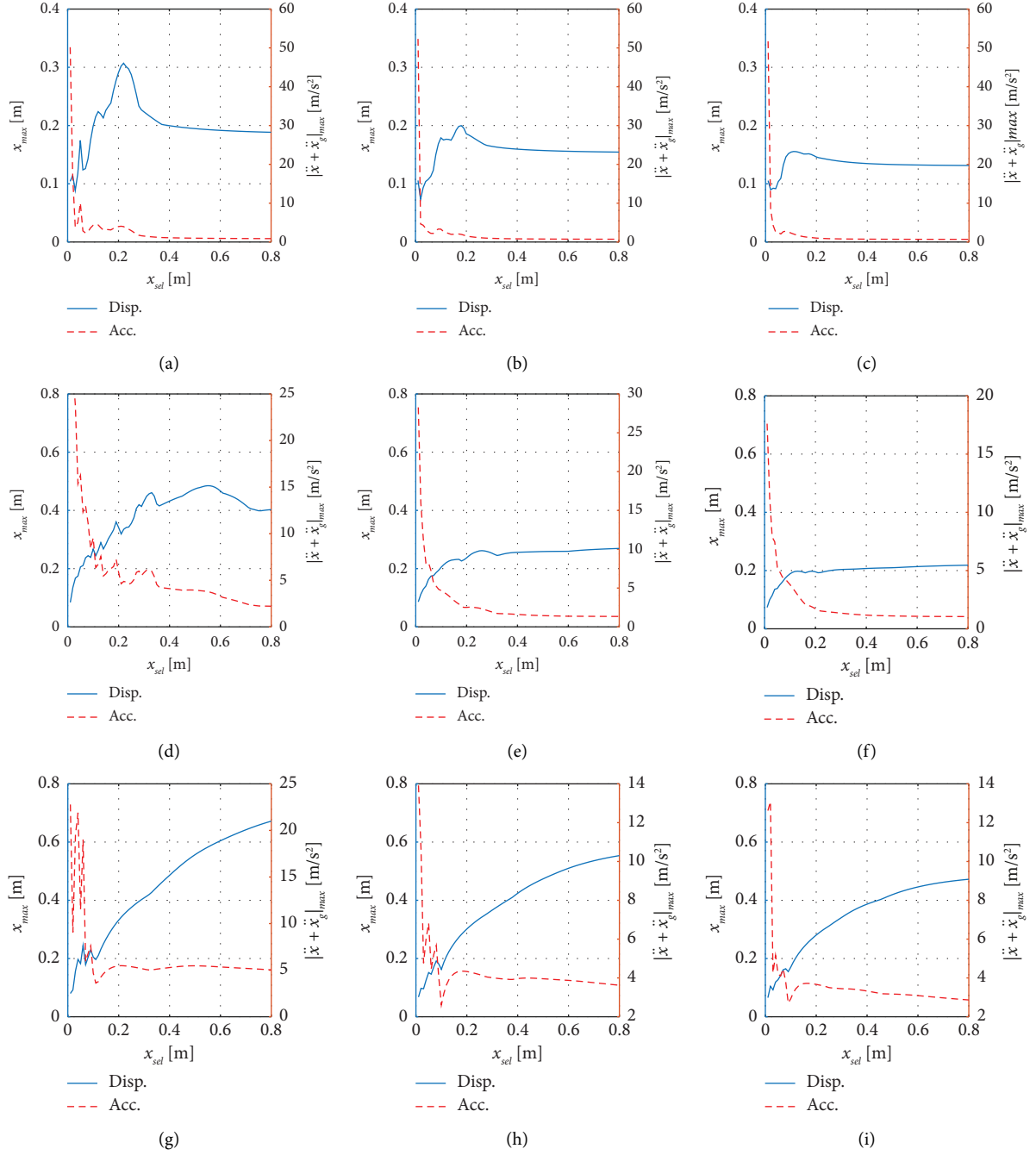
FIGURE 4: Maximum displacement and absolute acceleration of Duffing isolation models for several x_{sel} and damping ratios for Chi-Chi waves (CHY101-E) (a) $\xi = 0.04$, (b) $\xi = 0.10$, and (c) $\xi = 0.15$; Kobe waves (NIS000) (d) $\xi = 0.04$, (e) $\xi = 0.10$, and (f) $\xi = 0.15$; and random waves (g) $\xi = 0.04$, (h) $\xi = 0.10$, and (i) $\xi = 0.15$.

4.1. Experimental Setup. The specimen comprises a mass, which is assumed as a part of seismic isolation, four longitudinal linear springs, and a Duffing spring achieved by wire and disc springs (Figures 8 and 9(a)–9(e)). Note that since the mass is assumed to be a part of an actual seismic isolation system, the motion of the specimen is assumed as that of a real seismic isolation system.

As equation (4) shows that the coefficient of the Duffing spring is determined by the stiffness of the orthogonal spring, k_{ort}, a stiff spring is required to achieve a large Duffing-spring coefficient, Λ_{N3}. To achieve a stiff spring, this study used disc springs to make the Duffing spring. The Duffing spring device is shown in Figures 9(d) and 9(e). A wire connects the cylinder within the disc springs. The wire pulls the cylinder when

(a)

(b)

(c)

(d)
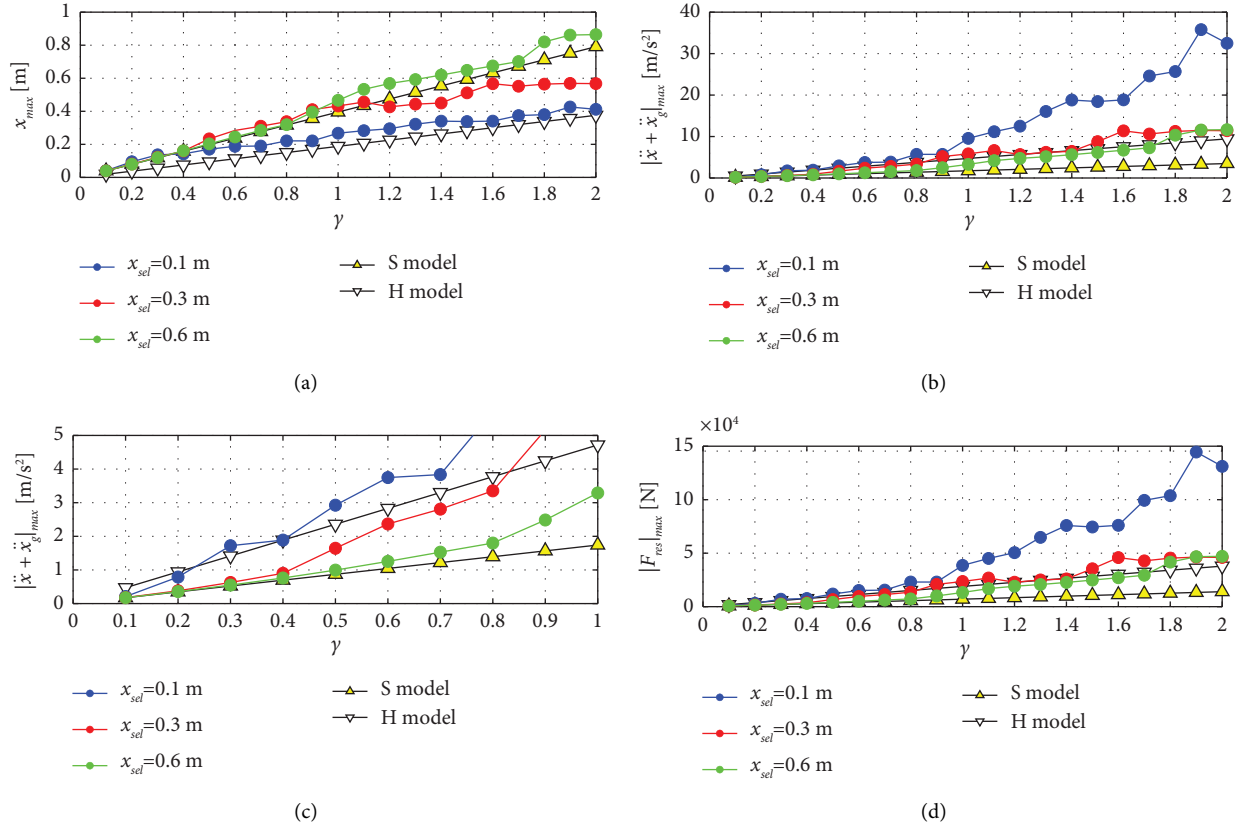
FIGURE 5: Relationship between γ and (a) maximum displacement, (b) maximum absolute acceleration, (c) enlargement of (b), and (d) restoring force ($T_s = 3.0$ s and $\xi = 0.04$).

the mass shakes. The cap then compresses the disc springs, and the disc springs apply the restoring force.

In this experiment, two load cells, one accelerometer, and one laser displacement meter are used. The load cells measure the restoring force of the Duffing spring. The accelerometer and the laser displacement meter measure the response of the mass. The load cell is placed on the top of the Duffing spring device, and the accelerometer and the target of the laser displacement meter are attached to the mass (Figures 8 and 9(a)). The wire transfers the restoring force of the disc springs to the mass and each load cell, which measures the tension of the wire. The length of the wire is 3.1 m ($d = 1.55$ m). The mass, (m), is 4038 kg, and the stiffness, k, is 13597 N/m. The value of k is chosen to achieve the natural period of standard seismic isolation. The damping ratio caused by friction (ξ) is estimated to be 0.04. The damping ratio is estimated by comparing and adjusting the results of the THA and experiment for sweep-up waves.

The clearance, which is the gap between the building and the surrounded retaining wall, of this specimen was 0.65 m that was determined by the clearance of seismic buildings in Japan [3].

This paper selected x_{sel} to be 0.3 m in equation (13) so that it can be the maximum displacement within the clearance. The wire length and the stiffness of the orthogonal

spring k_{ort} are 3.1 m and 439530 N/m, respectively, to achieve Λ_{N3} of 182947 N/m³, which is given by equation (4). Note that this Λ_{N3} is approximately the same with the value obtained from by equation (13) with $x_{sel} = 0.27$ m.

The vertical support of the mass is achieved by using a low-friction linear-roller-bearing system. The length of one guide is 4.4 m. The mass oscillates along the left and right directions as shown in Figure 9.

4.2. Experimental Results. This paper used two sweep waves represented by equation (24) as well as the random, El Centro, Hachinohe, and Kobe waves in the experiment. The random wave is an artificial wave, and the other three waves are measured waves.

(1) Sweep up (Figure 10): The amplitudes are 0.3, 0.2, 0.1, and 0.05 m/s² and the initial and target frequencies are 0.1 Hz and 1.2 Hz, respectively.

(2) Sweep down (Figure 11): The amplitudes are 0.3, 0.2, 0.1, and 0.05 m/s², and the initial and target frequencies are 1.2 Hz and 0.1 Hz, respectively.

(3) Random wave (Figure 2) is an artificial wave, and the pseudo velocity spectrum, $_pS_V$, is approximately 0.8 m/s for a structure with the natural period of longer than 0.64 s and damping ratio being 5%.
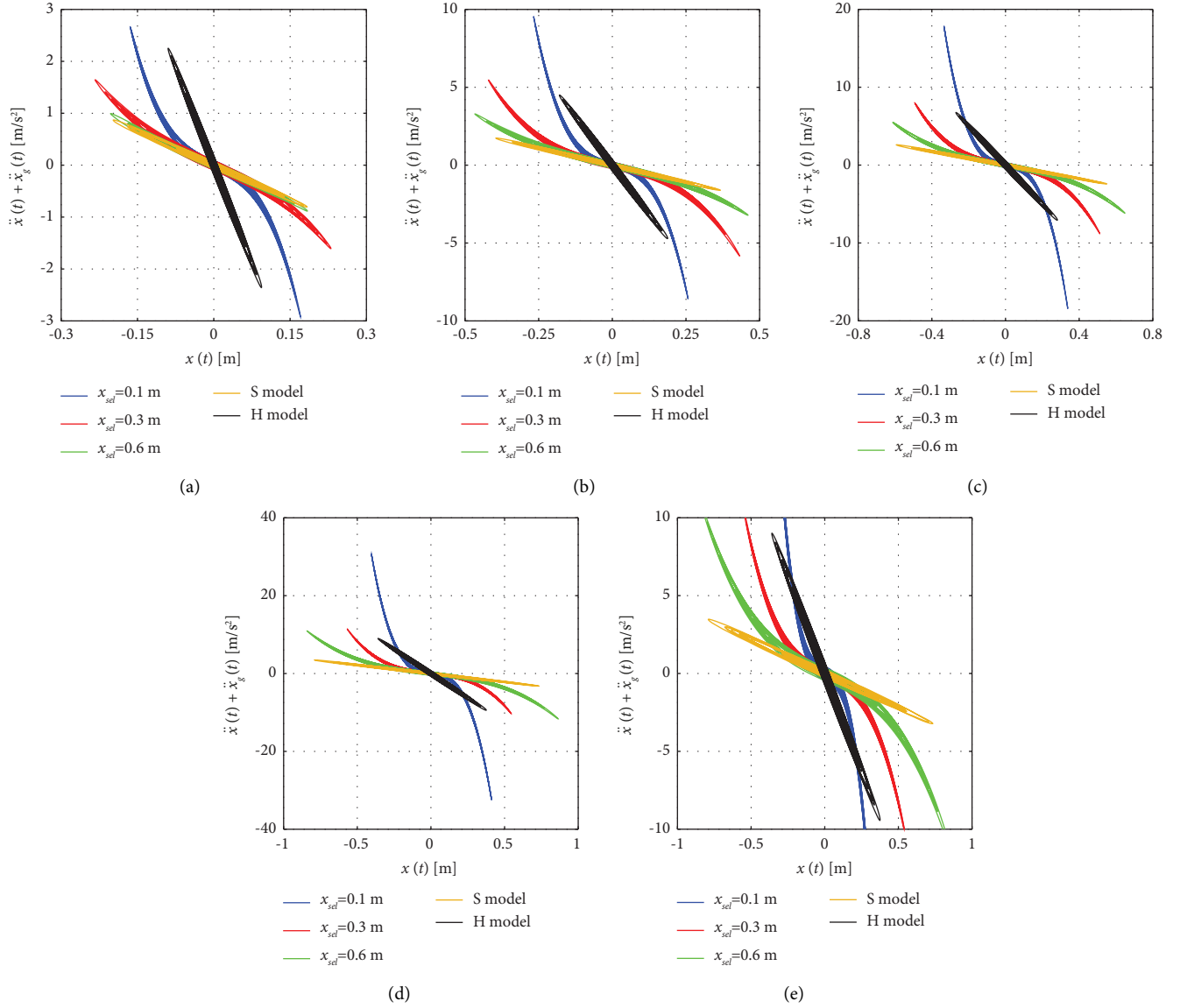
FIGURE 6: Comparison of Duffing isolation and linear systems for random waves with several γ: (a) $\gamma = 0.5$, (b) $\gamma = 1.0$, (c) $\gamma = 1.5$, (d) $\gamma = 2.0$, and (e) enlargement of (d) ($T_s = 3.0$ s and $\xi = 0.04$).

(4) El Centro wave, Imperial Valley earthquake of 1940.

(5) Hachinohe wave, Tokachi-Oki earthquake of 1968.

(6) Kobe wave, Great Hanshin earthquake of 1995.

To check the sinusoidal response of Duffing isolation, two sweep waves (sweep up and sweep down) are used:

$$\ddot{x}_g(t) = A_p \sin\left[2\pi f_{in} \frac{T\left(\eta^{t/T} - 1\right)}{\ln(\eta)}\right],$$

$$\eta = \frac{f_e}{f_{in}},$$

(24)

where A_p (m/s^2) is the amplitude of the wave, f_{in} (Hz) is the initial frequency, f_e (Hz) is the target frequency, and T (s) is the time length of the wave. The frequency of the signal $f_{sw}(t)$ (Hz) is given by

$$f_{sw}(t) = f_{in}\eta^{t/T}.$$

(25)

As equation (25) has shown that the frequency of the signal is a function of time, it varies continuously between f_{in} and f_e.

Figures 12 and 13 show the results of sweep-up waves, and Figures 14 and 15 show those of sweep-down waves. Figures 16 and 17 show the results of the random wave, Figures 18 and 19 show the results of the El Centro wave, Figures 20 and 21 show the results of the Hachinohe wave, and Figures 22 and 23 show the results of the Kobe wave. Figures 12(c) and 14(c) show the envelope curves of the sweep up and down waves.

Figures 12–23 compare the experimental and THA results. The THA results closely agree with the experimental results. The differences in 38 s and 50 s (Figure 16) are caused by the influence of nonlinear damping that depends on the response. Figure 12 shows the results of the
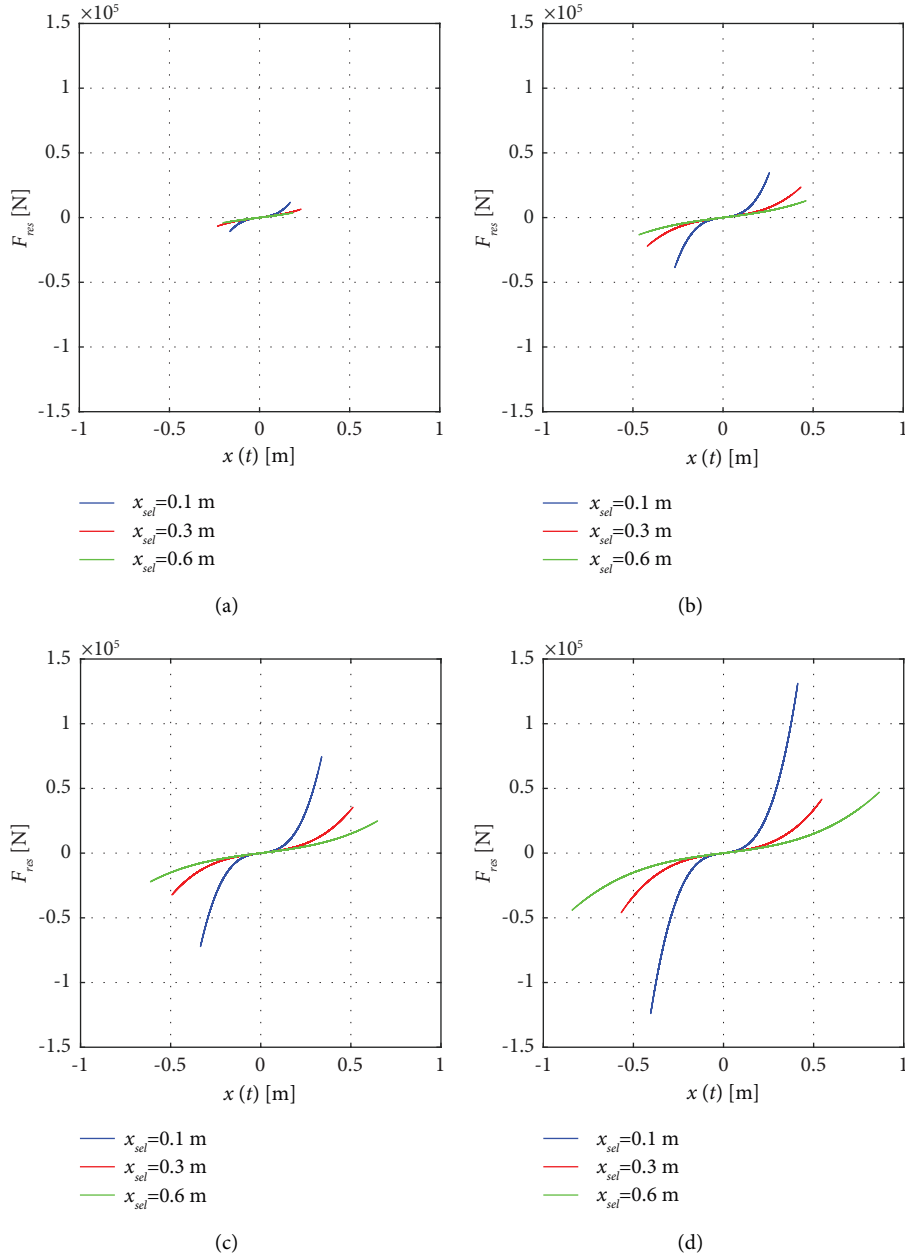
FIGURE 7: $F_{res}(t)$ of Duffing isolation for random waves with several γ: (a) $\gamma = 0.5$, (b) $\gamma = 1.0$, (c) $\gamma = 1.5$, and (d) $\gamma = 2.0$ ($T_s = 3.0$ s and $\xi = 0.04$).

estimation equations (12) and (18) with the parameters such as $\omega_s = 1.84$ rad/s, $\lambda_s = 39.3$ 1/(m²s²), and $\xi = 0.04$. The estimated maximum responses are close to the experimental and THA results. Table 1 shows and compares the results of the experiment (Exp.), time history analysis (THA), and estimation (Est.). Figures 12, 14, and 24 show that the response of Duffing isolation depends on the "direction" of an excitation frequency. In other words, the maximum displacements for the sweep-up and sweep-down waves are not the same, and the maximum

displacement for the sweep-up wave is bigger than that for the sweep-down waves. Figure 24 shows that $x(t)$ for sweep-up waves suddenly decreases at approximately 0.5 Hz ~ 0.6 Hz and $x(t)$ for sweep-down waves increases at approximately 0.35 Hz ~ 0.3 Hz. This behavior is known as the jump phenomenon that is caused by bifurcation.

Equations (12) and (18) estimate the maximum displacement and absolute acceleration for the sweep-up wave, respectively; and Figure 12 includes the estimated
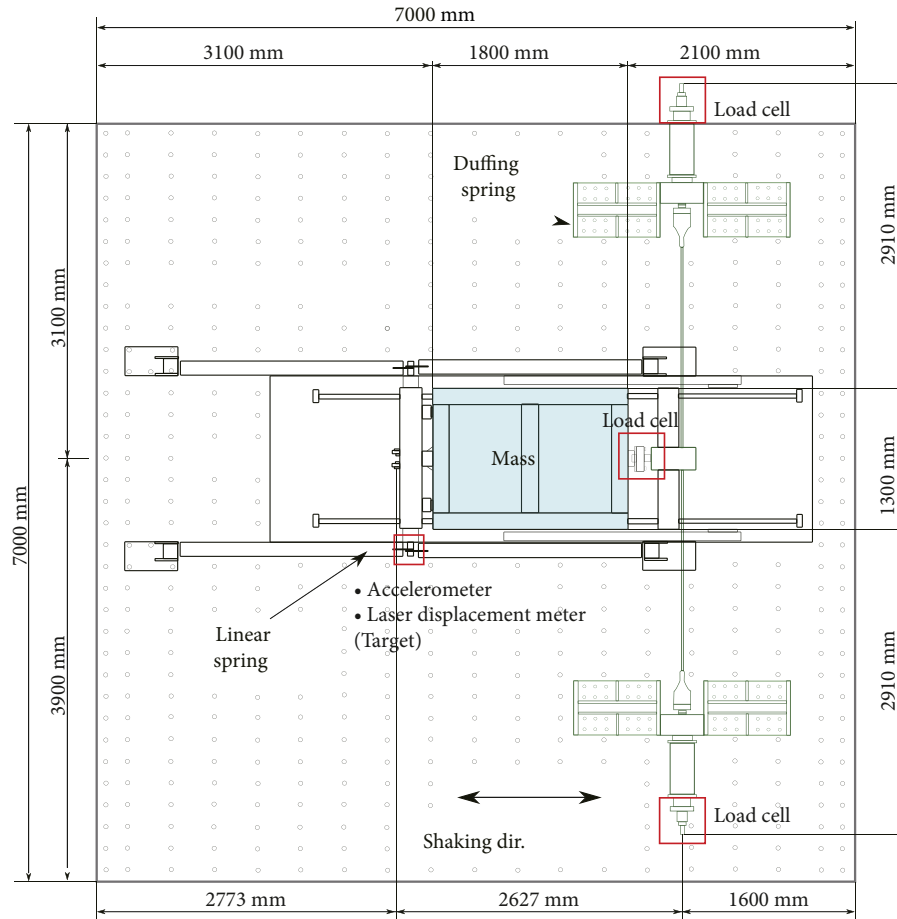
FIGURE 8: Specimen of Duffing isolation.

results. This implies that if an excitation frequency varies from low to high levels, the response amplitude increases to r_p. However, if an excitation frequency decreases, the maximum amplitude is lower than r_p (Figure 24). The reason is that Duffing isolation is one of the hardening systems, and the frequency at the maximum response is higher than that of the linear system. Thus, the backbone curve bends to the right side in the frequency space with an excitation intensity increase, and it causes branches. The stable upper branch of the response curve is found for the sweep-up wave despite the fact that the stable lower branch of the response curve is found for the sweep-down wave. Figure 24 shows the envelope curves of the maximum displacement and $f_{sw}(t)$ for sweep-up and sweep-down waves. Equation (12) estimates the maximum displacement for the resonant branch, and the estimated value is close to the result for sweep-up waves. To reduce the maximum displacement for the wave with the dominant frequency that varies from low to high such as the sweep-up wave, a possible solution would be to increase the damping ratio.

Figure 7 shows that the restoring force of the Duffing spring increases sharply as the displacement increases to suppress the maximum displacement. The same fact can be seen in the experimental results (Figures 13(b), 15(b), 17(b), 19(b), 21(b), and 23(b)).

Figure 25 compares the experimental results of the Duffing isolation and S models. These results show that the displacement and absolute acceleration of the Duffing isolation and S models are approximately the same for $x(t) < 0.2$ m. On the other hand, the absolute acceleration of Duffing isolation increases shapely because the Duffing spring applies a strong restoring force. This is the same trend as observed in Figure 3(c).

Next, the influence of the disturbance amplitude on the responses is assessed. As aforementioned, the restoring force of the Duffing spring depends on the displacement. Thus, the dynamic behavior depends on the disturbance apmlitude. To verify, this section compares the experimental results of the S and Duffing isolation models for sweep waves with different amplitudes.

Figures 26 and 27 show that the relationship between the acceleration and displacement of the S model is linear even if the disturbance amplitude becomes large. In contrast, the relation for the Duffing isolation model is not linear. This is because the restoring force of the Duffing spring depends on the cube of the displacement.
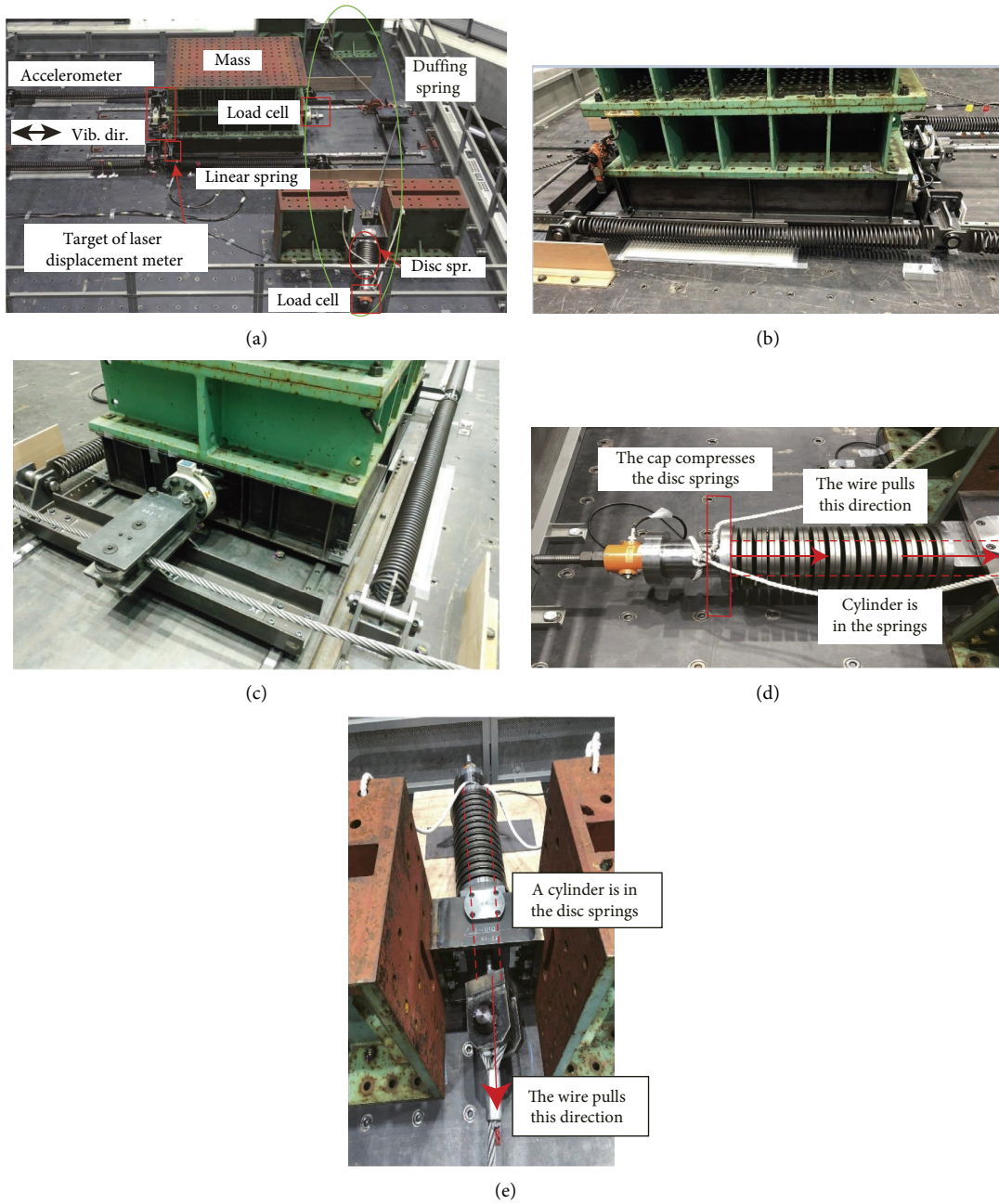
(a)

(b)

(c)

(d)

(e)

FIGURE 9: Specimen: (a) specimen overview, (b) linear springs, (c) wires of Duffing springs, (d) disc springs, and (e) connection between wire and disc springs.

Figures 26 and 27 also show that the maximum responses of the Duffing isolation model for sweep-up and sweep-down waves are not the same. However, the responses for them are almost the same for the S model. This is the same trend as observed in Figure 24. Figure 28 compares the frequency, $f_{sw}(t)$ (Hz), of the sweep waves and the natural frequency, $f_{str}(t)$ (Hz), of the Duffing isolation model, which is given by

$$f_{str}(t) = \frac{1}{2\pi}\sqrt{\frac{k_{all}(x(t))}{m}}$$

$$= \frac{1}{2\pi}\sqrt{\frac{k + \Lambda_{N3}x^2(t)}{m}}.$$

(26)
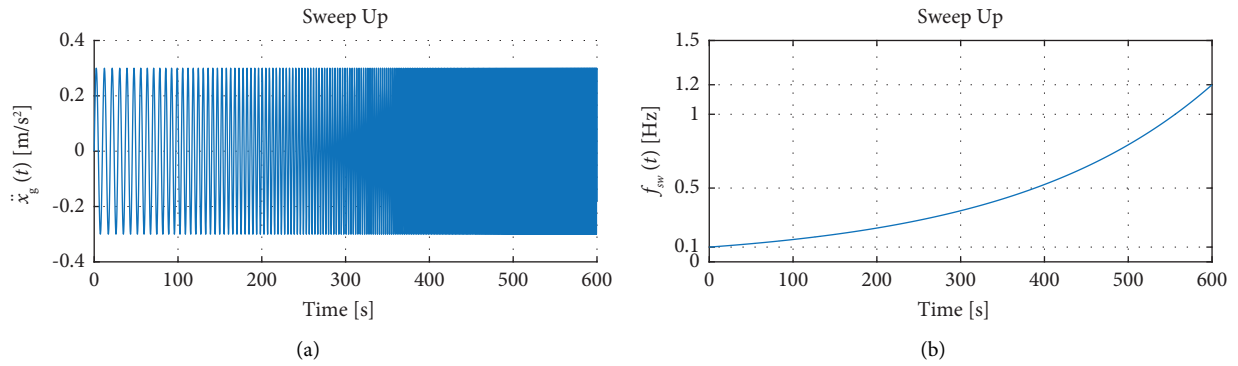
Figure 10: Sweep-up wave: (a) accelerogram and (b) dominant frequency vs. time ($A_p = 0.3 \, \text{m/s}^2$).
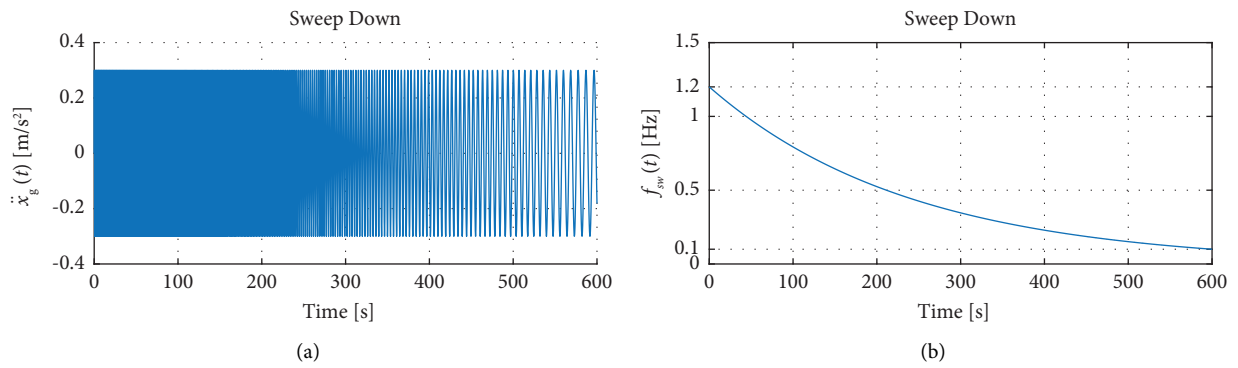
Figure 11: Sweep-down wave: (a) accelerogram and (b) dominant frequency vs. time ($A_p = 0.3 \, \text{m/s}^2$).
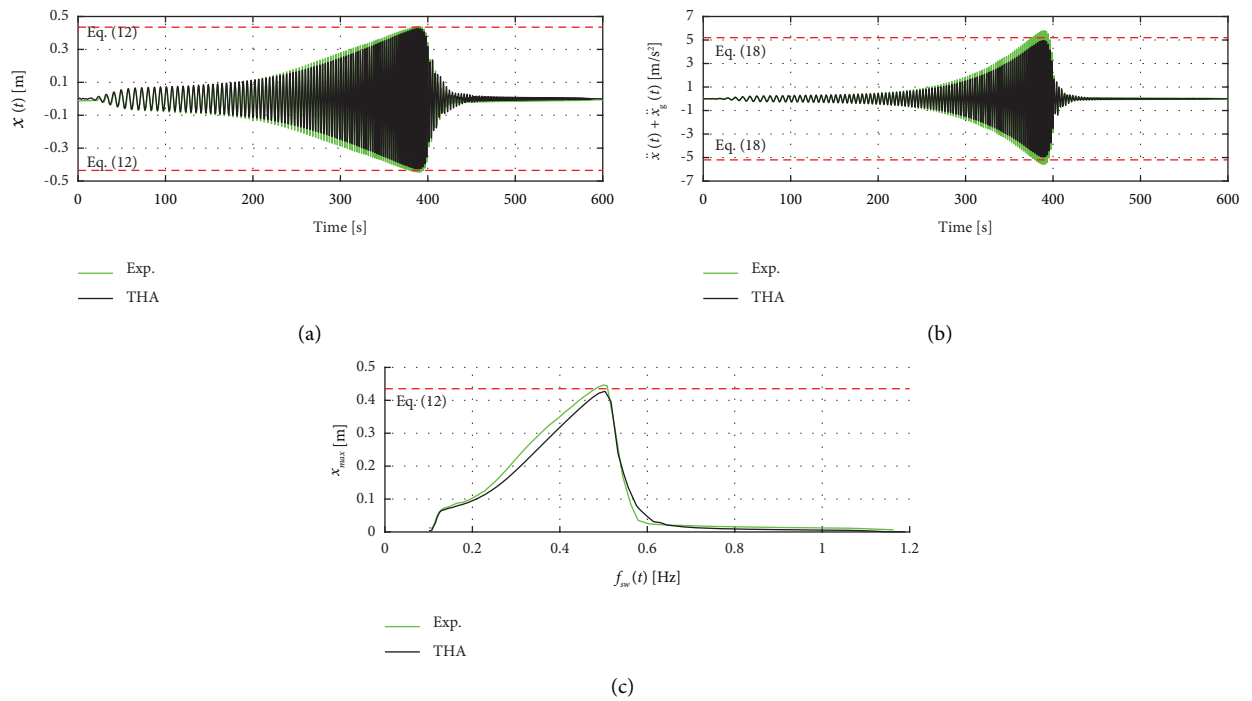
Figure 12: Responses for sweep-up wave: (a) displacement, (b) absolute acceleration, and (c) envelope curves of $x_{\max}$ vs. $f_{sw}(t)$ ($A_p = 0.3 \, \text{m/s}^2$).

(a)

(b)
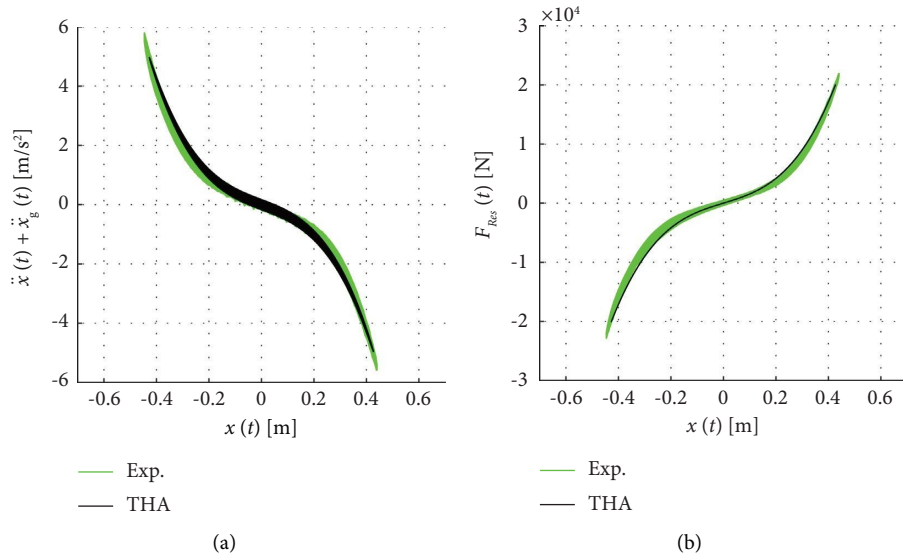
FIGURE 13: Comparison between the THA and experimental results for sweep-up wave: (a) absolute acceleration vs. displacement and (b) restoring force of Duffing isolation vs. displacement ($A_p = 0.3\,\text{m/s}^2$).


(a)

(b)

(c)
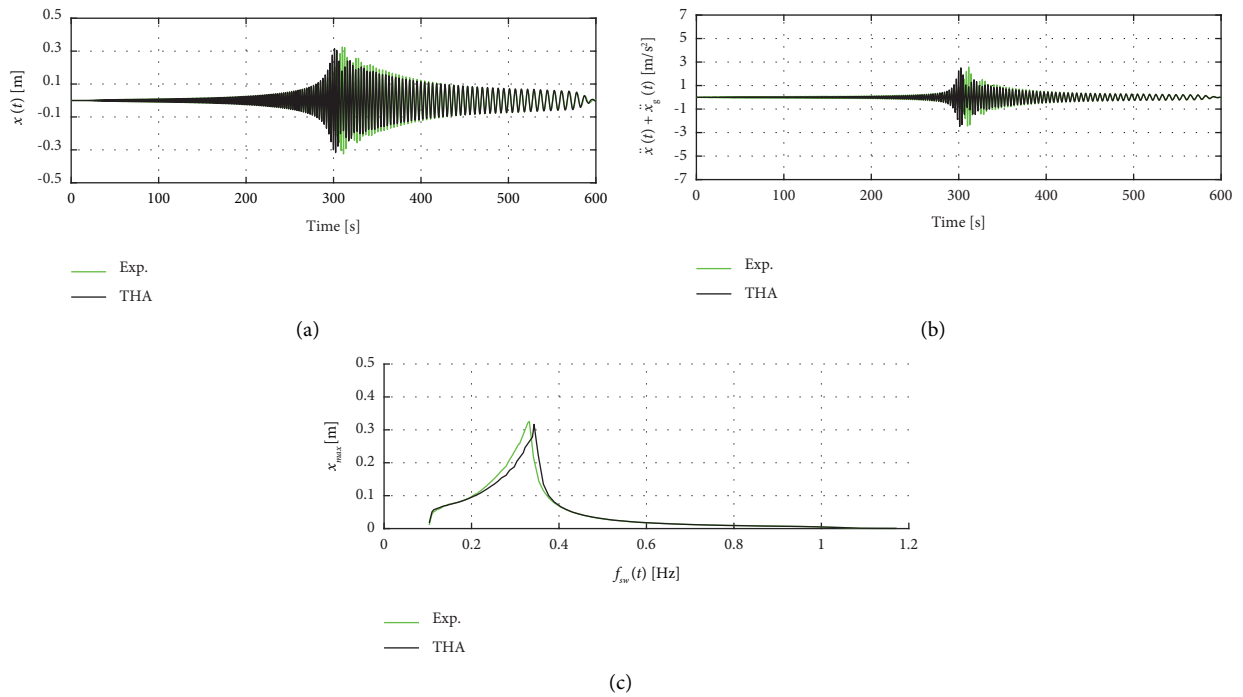
FIGURE 14: Responses for sweep-down wave: (a) displacement, (b) absolute acceleration, and (c) envelope curves of $x_{\max}$ vs. $f_{sw}(t)$ ($A_p = 0.3\,\text{m/s}^2$).

Figure 28 shows that both $f_{sw}(t)$ and $f_{str}(t)$ increase until 400 s for the sweep-up wave causing large responses. In contrast, for the sweep-down wave, although $f_{sw}(t)$ decreases, the natural frequency, $f_{str}(t)$, increases with time until $f_{str}(t)$ takes the peak value. This result explains the reasons that the responses of the Duffing isolation model depend on the direction of the frequency of the input wave.
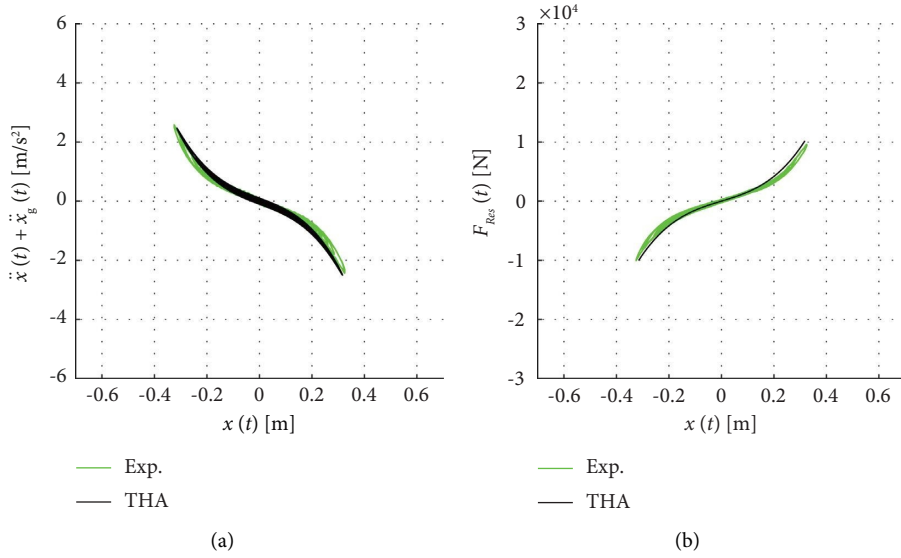
FIGURE 15: Comparison between the THA and experimental results for sweep-down wave: (a) absolute acceleration vs. displacement and (b) restoring force of Duffing isolation vs. displacement ($A_p = 0.3 \, \text{m/s}^2$).
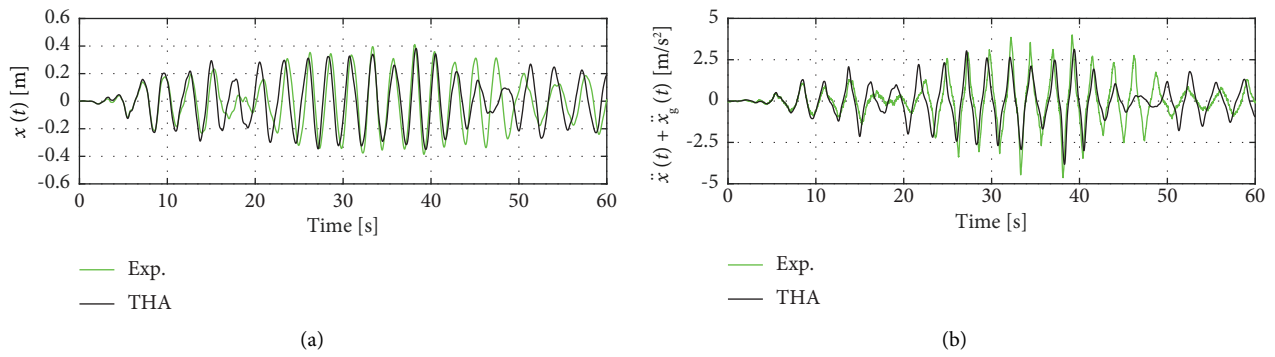
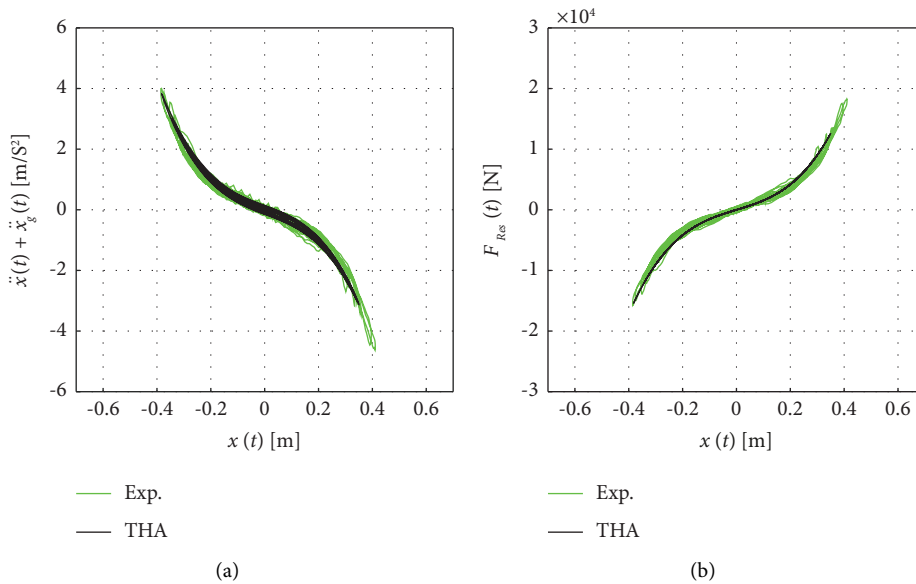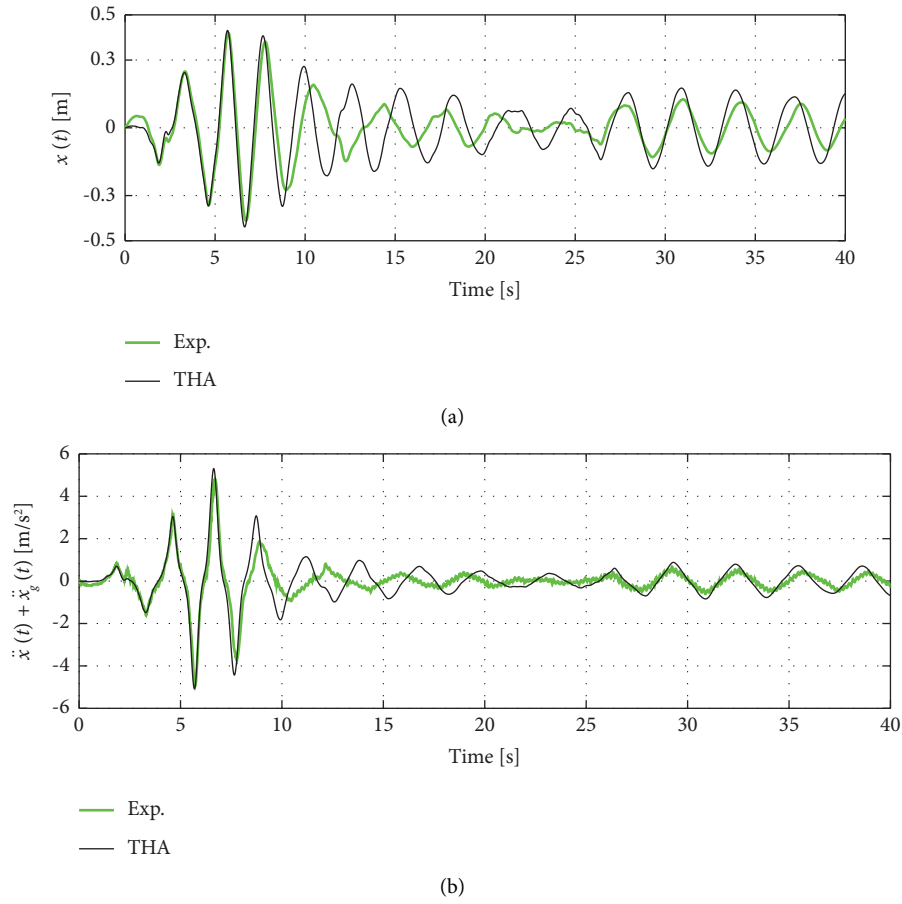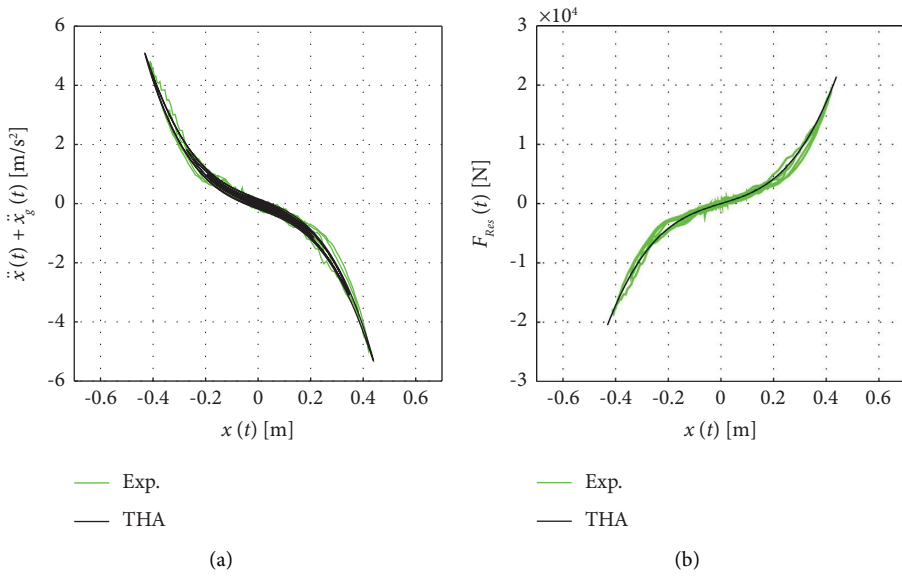FIGURE 16: Responses for random wave: (a) displacement and (b) absolute acceleration.

FIGURE 17: Comparison between the THA and experimental results for random wave: (a) absolute acceleration vs. displacement and (b) restoring force of Duffing isolation vs. displacement.

(a)
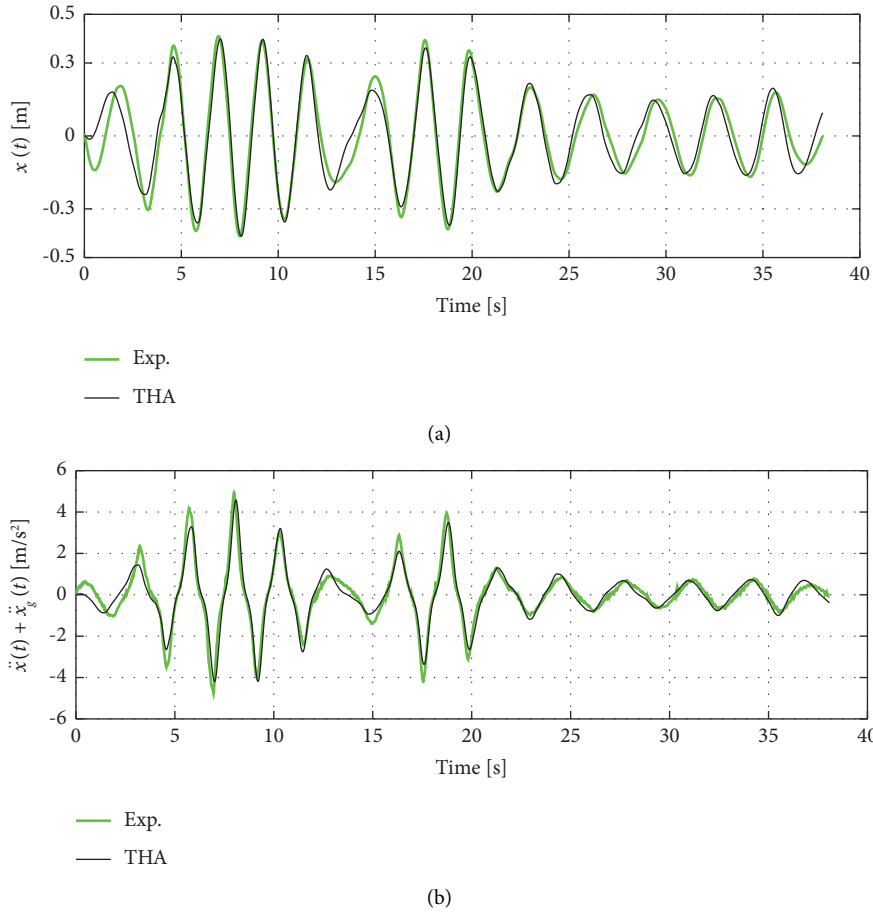

(b)

Figure 18: Responses for El Centro wave: (a) displacement and (b) absolute acceleration.

(a)

(b)

Figure 19: Comparison between the THA and experimental results for El Centro wave: (a) absolute acceleration vs. displacement and (b) restoring force of Duffing isolation vs. displacement.

FIGURE 20: Responses for Hachinohe wave: (a) displacement and (b) absolute acceleration.
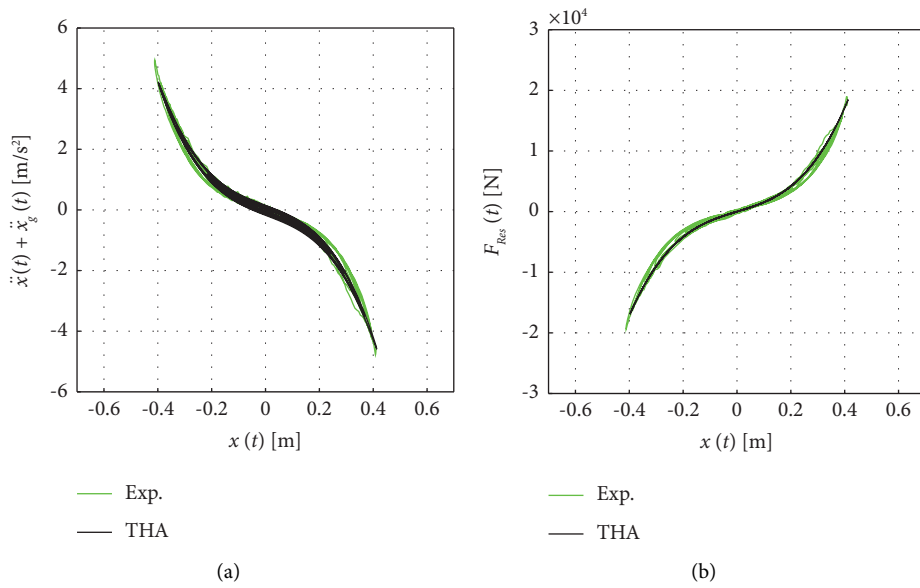

FIGURE 21: Comparison between the THA and experimental results for Hachinohe wave: (a) absolute acceleration vs. displacement and (b) restoring force of Duffing isolation vs. displacement.
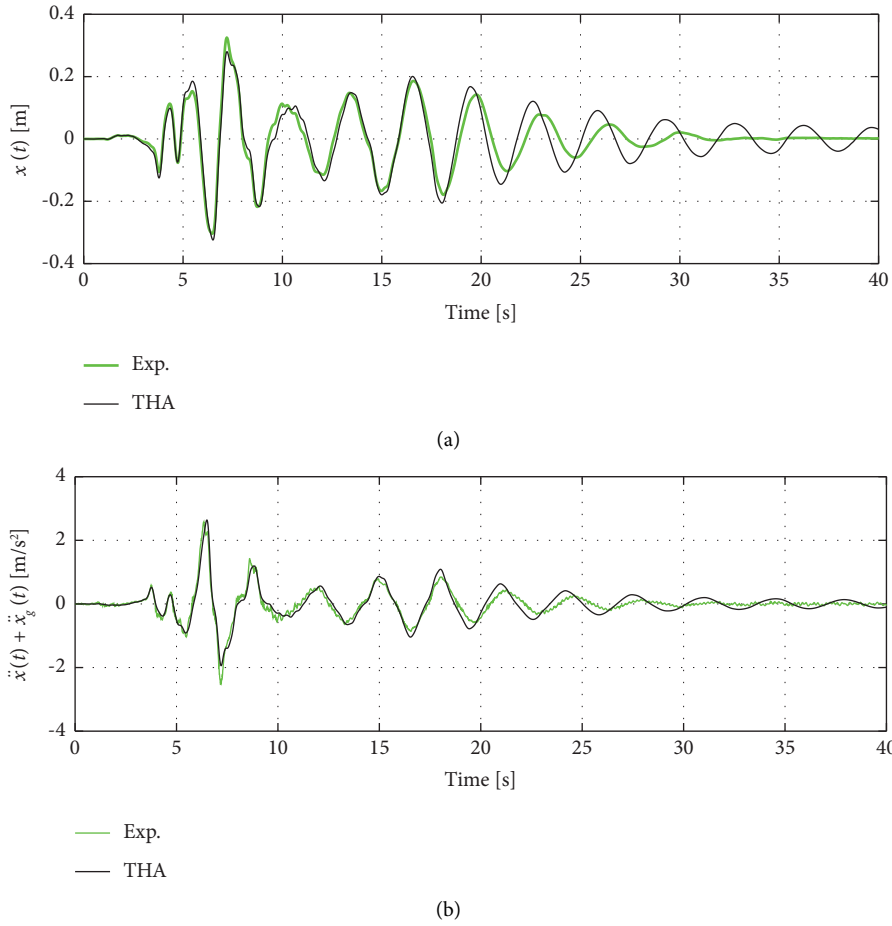
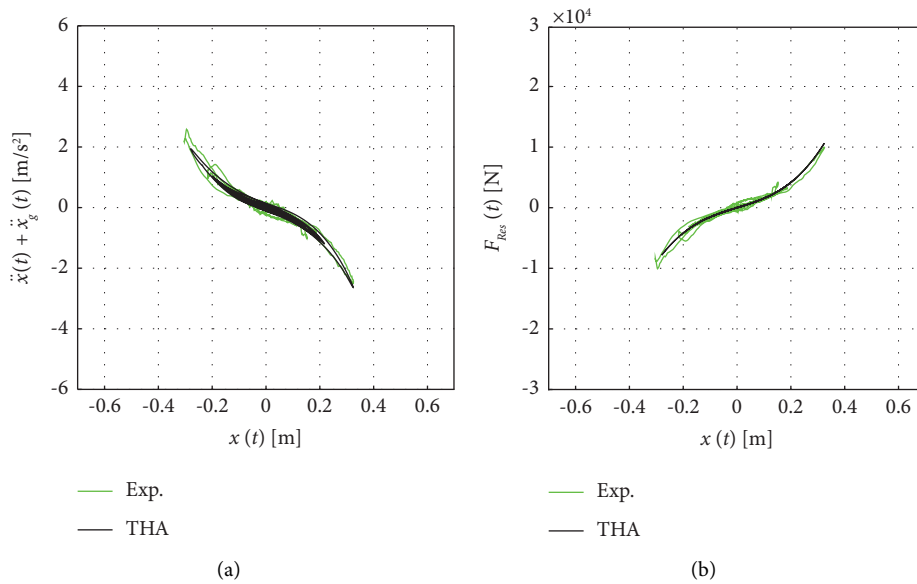FIGURE 22: Responses for Kobe wave: (a) displacement and (b) absolute acceleration.

FIGURE 23: Comparison between the THA and experimental results for Kobe wave: (a) absolute acceleration vs. displacement and (b) restoring force of Duffing isolation vs. displacement.

TABLE 1: Comparison among maximum responses of the experiment, THA, and estimation for sweep up waves.

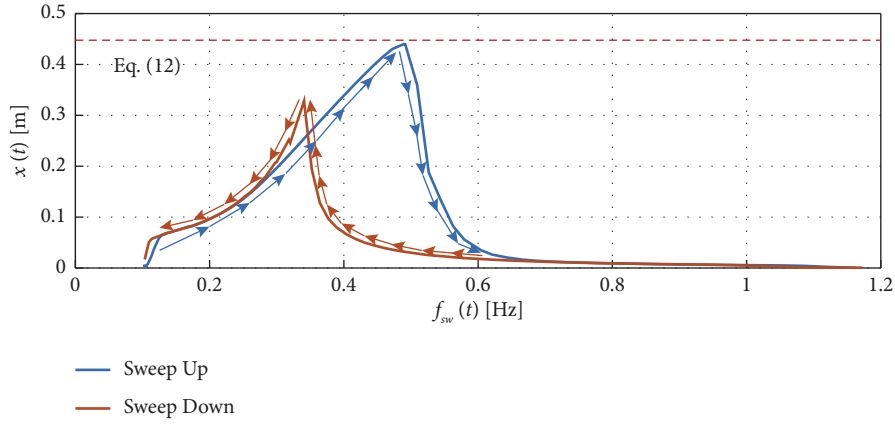|	Exp.	THA	Est. (equations (12) and (18))	Exp./Est. (%)	THA/Est. (%)
$x_{\max}$ (m)	0.44	0.43	0.44	98.3	98.1
$|\ddot{x} + \ddot{x}_g|_{\max}$ (m/s^2)	5.79	4.97	5.20	111.3	95.5

FIGURE 24: Envelope curves for sweep-up and sweep-down waves ($A_p = 0.3$ m/s^2) (experimental results).
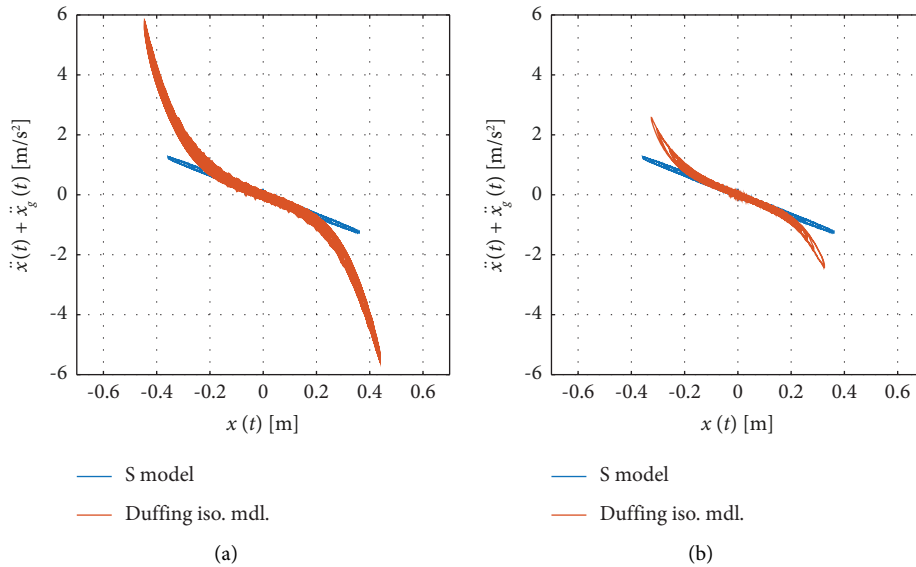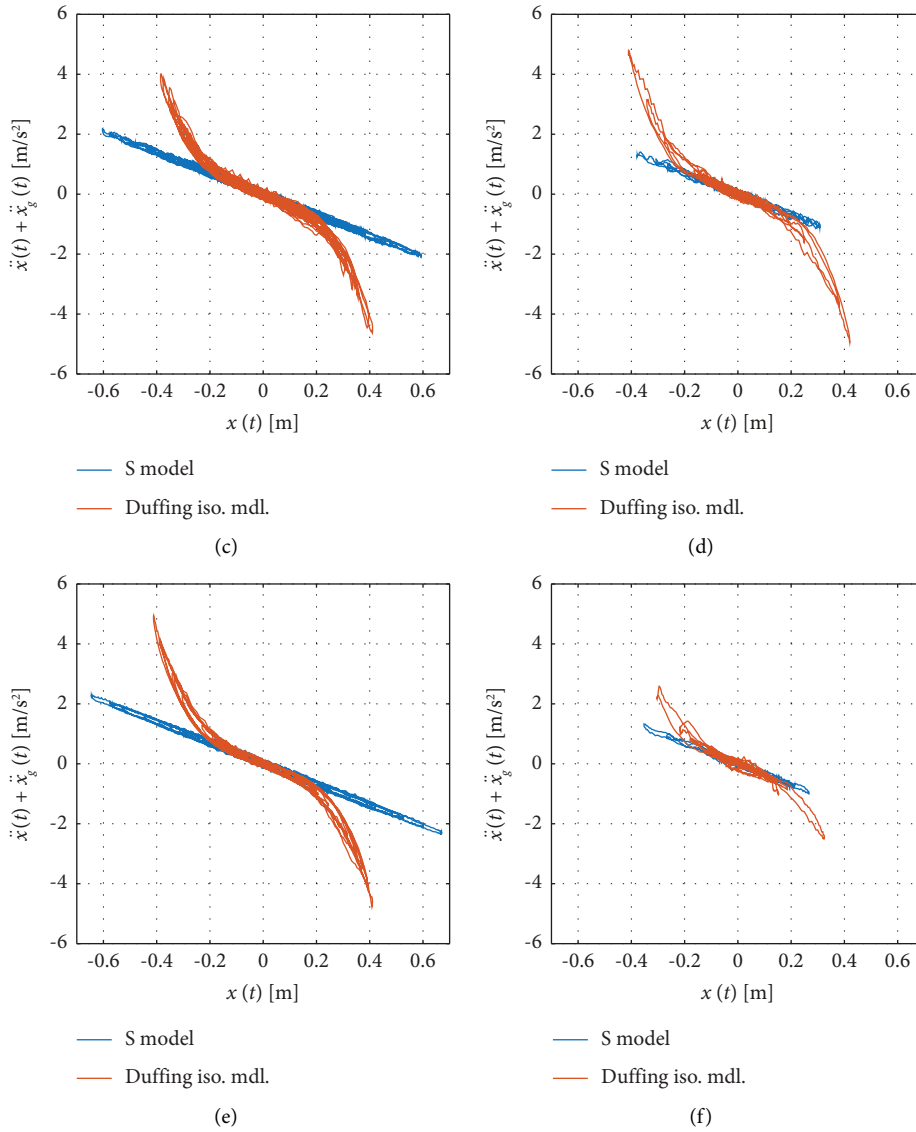

(a)

(b)

FIGURE 25: Continued.

FIGURE 25: Comparison of the results of experiments of the S model (w/o Duffing springs) and the Duffing isolation model for sweep waves: (a) sweep up ($A_p = 0.3$ m/s²), (b) sweep down ($A_p = 0.3$ m/s²), (c) random wave, (d) El Centro wave, (e) Hachinohe wave, and (f) Kobe wave (experimental results).
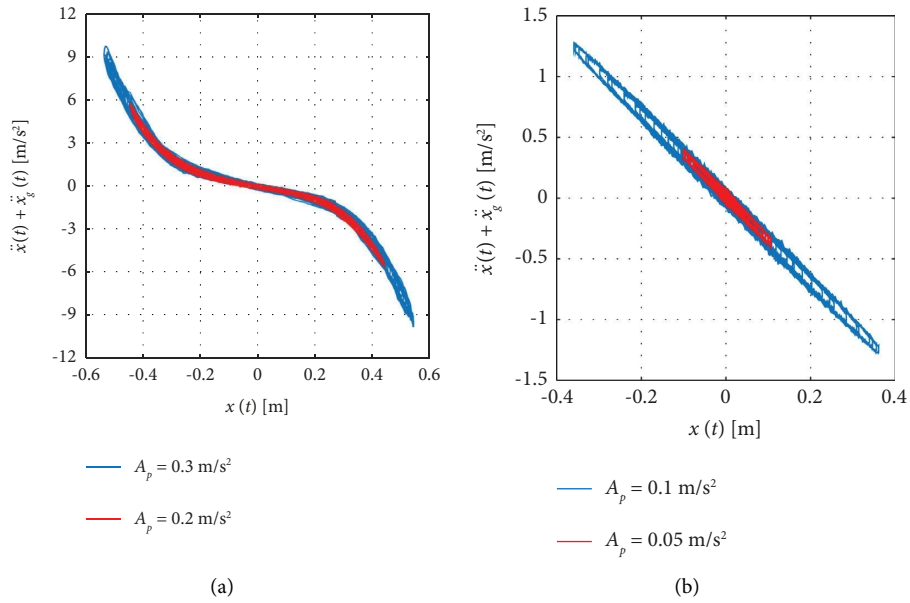
FIGURE 26: Comparison of responses for different amplitudes of sweep-up waves: (a) with the Duffing spring and (b) without the Duffing spring (experimental results).
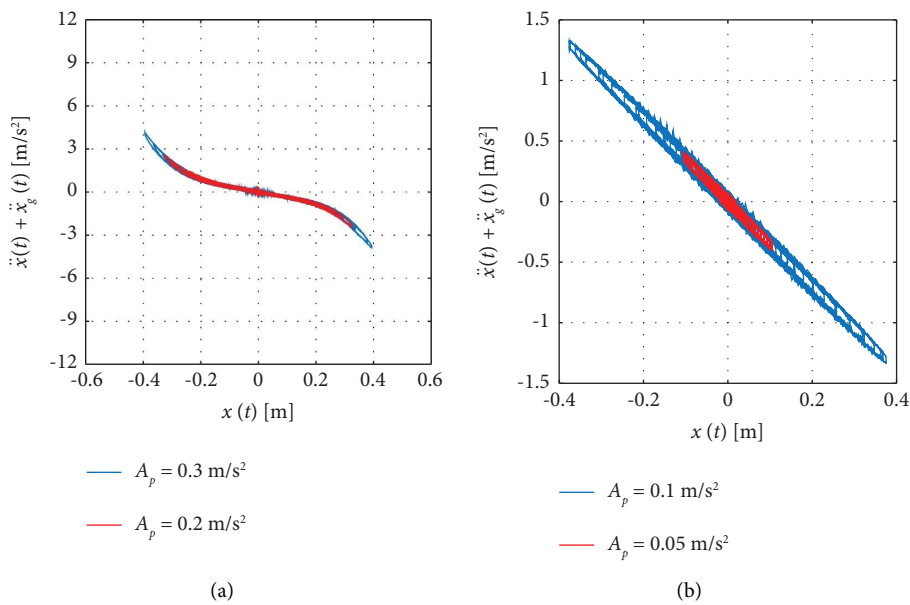

FIGURE 27: Comparison of responses for different amplitudes of sweep-down waves: (a) with the Duffing spring and (b) without the Duffing spring (experimental results).
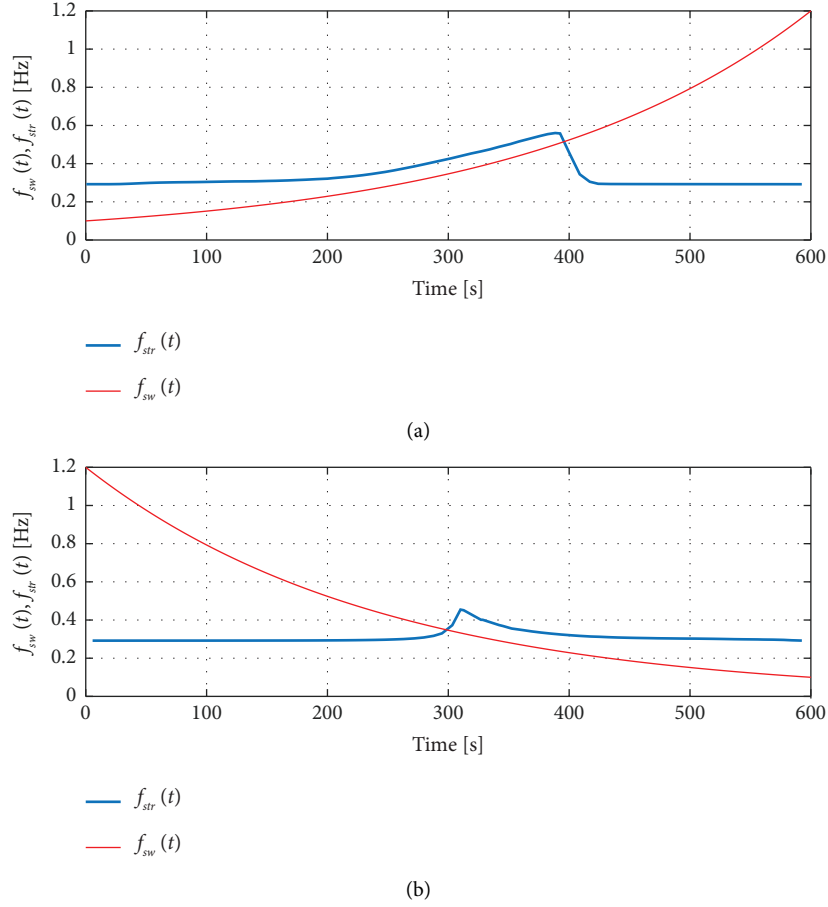
(a)

(b)

FIGURE 28: Comparison of frequency of sweep waves and natural frequency of the Duffing isolation model: (a) sweep up and (b) sweep down ($A_p = 0.3\,\text{m/s}^2$) (experimental results).

5. Conclusion

This paper developed seismic isolation with a Duffing spring with its restoring force given by the cube of the displacement. This study also revealed the influence of the coefficient of the Duffing spring. Furthermore, to verify the advantage of Duffing isolation, this paper devised a way to implement a Duffing spring for seismic isolation and conducted an experiment. This paper clarified the following points:

(i) This paper presented a way to determine the coefficient of the Duffing spring with the selected displacement, x_{sel}. The small x_{sel} gives a large coefficient of the Duffing spring, and large x_{sel} gives its small coefficient.

(ii) The Duffing spring with small x_{sel} results in small displacements but in large absolute acceleration. In contrast, large x_{sel} results in a large displacement and small absolute acceleration.

(iii) As the stiffness of the Duffing spring depends on the displacement of the structure, the amplitude of the input wave influences the stiffness of Duffing isolation.

(iv) This paper devised a way to implement the Duffing spring, and the Duffing spring can be achieved by using a wire and disc springs.

(v) The comparison of the experimental and THA results showed that the THA results are in close agreement with the experimental results and that the validity of the Duffing spring was verified in an actual system.

(vi) The experimental results also showed that the behavior of the Duffing isolation and seismic isolation models is almost the same for small displacements. In contrast, since the stiffness of the Duffing spring increases with a large displacement, Duffing isolation suppresses the maximum displacement for large waves.

This study is the first step in applying a Duffing spring to seismic isolation. The numerical model does not include nonlinear damping. However, an actual system contains nonlinear damping, and reflecting its effects is one of the future works.

Note that this paper is a continuation of the following preprint [22].

Abbreviations:

DOF: Degree-of-freedom
H model: Linear model with a stiff spring
Duffing isolation: Seismic isolation, which stiffness is soft, with the Duffing spring
Duffing spring: A spring whose restoring force is given by equation (4)
S model: Linear model with a soft spring
THA: Time history analysis.

Appendix

A. Polynomial Approximation of $F_n(x(t))$

This section explains the derivation of $F_n(x(t))$. The consideration of polynomial approximation is explained.

A.1. Derivation of $F_n(x(t))$. As shown in Figure 1, the restoring force of the Duffing spring, $F_n(t)$, (equation (2)), is given by

$$F_n(x(t)) = 2k_{ort}\left(1 - \frac{d_0}{\sqrt{x^2(t) + d^2}}\right)x(t). \quad (A.1)$$

Carrella et al. showed that the restoring force of the Duffing spring can be described by the Taylor polynomial of approximation [23], and usually, its third Taylor polynomial is used (e.g., [9, 10, 23]). The third Taylor polynomial of the restoring force, $F_n(x)$, is

$$F_n(x(t)) = F_n(0) + \frac{F_n^{(1)}(0)}{1!}x(t) + \frac{F_n^{(2)}(0)}{2!}x^2(t) + \frac{F_n^{(3)}(0)}{3!}x^3(t),$$
$$(A.2)$$

where $F_n^{(N)}(x(t))$ is the N-th derivative of $F_n(x(t))$ based on $x(t)$. In particular, if $d = d_0$, $F_n^{(1)}(0)$, $F_n^{(2)}(0)$, and $F_n^{(3)}(0)$ are given as follows:

$$F_n^{(1)}(0) = 0,$$

$$F_n^{(2)}(0) = 0, \quad (A.3)$$

$$F_n^{(3)}(0) = 6k_{ort}\frac{1}{d_0^2}.$$

A.2. Influence of High-Order Terms. Next, the polynomial approximation for the Duffing spring is considered.

Regrouping equation (A.1) yields the following equation:

$$F_n(x(t)) = 2k_{ort}\left(1 - \frac{d_0}{\sqrt{x^2(t) + d^2}}\right)x(t), \quad (A.4)$$

$$= 2k_{ort}\left(d - d_0 + d_0 - \frac{d_0}{\sqrt{(x(t)/d^2 + 1}}\right)$$
$$\cdot \left(\frac{x(t)}{d}\right), \quad (A.5)$$

$$= 2k_{ort}(d - d_0)\left(\frac{x(t)}{d}\right)$$
$$+ 2k_{ort}d_0\left(1 - \frac{1}{\sqrt{(x(t)/d^2 + 1}}\right)\left(\frac{x(t)}{d}\right). \quad (A.6)$$

If $|x(t)/d| < 1$, then $1/\sqrt{(x(t)/d^2 + 1}$ can be approximated by using the binomial series:

$$\frac{1}{\sqrt{(x(t)/d^2 + 1}} = \sum_{j=0}^{\infty} {}_{(1/2)}C_j\left(\frac{x(t)}{d}\right)^{2j}, \quad (A.7)$$

$$= 1 - \frac{1}{2}\left(\frac{x(t)}{d}\right)^2 + \frac{3}{8}\left(\frac{x(t)}{d}\right)^4 - \frac{5}{16}\left(\frac{x(t)}{d}\right)^6 + \cdots. \quad (A.8)$$

In the aforementioned equation, ${}_mC_n$ indicates a combination of m and n:

$$_mC_n = \frac{m(m-1)(m-2)\cdots(m-n+1)}{n!}. \quad (A.9)$$

Substituting (A.8) into (A.6) yields

$$F_n(x(t)) = 2k_{ort}(d - d_0)\left(\frac{x(t)}{d}\right) + 2k_{ort}d_0\left[\frac{1}{2}\left(\frac{x(t)}{d}\right)^2 - \frac{3}{8}\left(\frac{x(t)}{d}\right)^4 + \cdots\right]\left(\frac{x(t)}{d}\right)$$
$$(A.10)$$
$$= 2k_{ort}(d - d_0)\left(\frac{x(t)}{d}\right) + k_{ort}d_0\left(\frac{x(t)}{d}\right)^3 - \frac{3}{4}k_{ort}d_0\left(\frac{x(t)}{d}\right)^5 + \cdots.$$

In particular, if $d = d_0$, $F_n(x(t))$ can be approximated as

$$F_n(x(t)) = k_{ort}d_0\left(\frac{x(t)}{d_0}\right)^3 - \frac{3}{4}k_{ort}d_0\left(\frac{x(t)}{d_0}\right)^5 + \cdots.$$
$$(A.11)$$

Note that $F_n^{(N)}(0)/N!$, which is the coefficient of $x^N(t)$ in the Taylor polynomial series, is the same as the coefficient of $(x(t)/d_0)^N$ multiplied by d_0^{-N}.

This is worth mentioning that if $|x(t)/d_0| > 1$, the value of the approximation will not converge. In other words, the restoring force of the Duffing spring can be approximated if the displacement, $x(t)$, is smaller than d_0.

The Duffing oscillator includes both a Duffing spring and a linear spring. Figures 13, 15, 17, 19, 21, and 23 compare the results of the THA and experiment of the restoring force of the Duffing spring system. The comparison demonstrated that the combination of a third-order polynomial equation and a linear spring component appropriately approximates the restoring force of the Duffing oscillator in this paper.

Data Availability

The data used to support the findings of this study are available from the corresponding author upon reasonable request.

Conflicts of Interest

The authors declare that they have no conflicts of interest.

Authors' Contributions

Kou Miyamoto wrote the original draft and conducted the experiment and analysis. Jun Iba conducted the experiment and data curation. Koichi Watanabe planned and conducted the experiment. Ken Ishii supervised and derived theories and equations. Masaru Kikuchi supervised all experiments and analysis.

Acknowledgments

References

[1] J. P. D. Hartog, *Mechanical Vibrations*, Dover, Illinois, IL, USA, 1985.

[2] N. Makris, "Seismic isolation: early history," *Earthquake Engineering & Structural Dynamics*, vol. 48, no. 2, pp. 269–283, 2019.

[3] M. Higashino and S. Okamoto, *Response Control and Seismic Isolation of Buildings*, Routledge, England, UK, 2006.

[4] K. K. Walsh, G. Sallar, J. T. Haftman, and E. P. Steinberg, "Resetting passive stiffness damper with passive negative stiffness device for seismic protection of structures," *Structural Control and Health Monitoring*, vol. 28, no. 8, 2021.

[5] C. Masnata, A. Di Matteo, C. Adam, and A. Pirrotta, "Assessment of the tuned mass damper inerter for seismic response control of base-isolated structures," *Structural Control and Health Monitoring*, vol. 28, no. 2, 2021.

[6] L. Li and Q. Liang, "Effect of inerter for seismic mitigation comparing with base isolation," *Structural Control and Health Monitoring*, vol. 26, no. 10, 2019.

[7] P. Bin, M. H. Tehrani, M. Nisa, P. S. Harvey, and A. A. Taflanidis, "Analysis and optimization of a nonlinear

[8] dual-mode floor isolation system subjected to earthquake excitations," *Earthquake Engineering & Structural Dynamics*, vol. 50, no. 9, pp. 2334–2354, 2021.

[8] D. M. Fenz and M. C. Constantinou, "Spherical sliding isolation bearings with adaptive behavior: theory," *Earthquake Engineering & Structural Dynamics*, vol. 37, no. 2, pp. 163–183, 2008.

[9] I. Kovacic and M. J. Brennan, Eds., *The Duffing Equation: Nonlinear Oscillators and Their Behavior*, Wiley, New York, NY, USA, 2011.

[10] A. Carrella, M. J. Brennan, and T. P. Waters, "Force transmissibility of a nonlinear vibration isolator with high-static-low-dynamic stiffness," in *Proceedings of the 6th EUROMECH Nonlinear Dynamics Conference ENOC 2008*, Saint Petersburg, Russia, June, 2008.

[11] G. Dong, Y. Zhang, Y. Luo, S. Xie, and X. Zhang, "Enhanced isolation performance of a high-static-low-dynamic stiffness isolator with geometric nonlinear damping," *Nonlinear Dynamics*, vol. 93, no. 4, pp. 2339–2356, 2018.

[12] B. Yan, H. Ma, B. Jian, K. Wang, and C. Wu, "Nonlinear dynamics analysis of a bi-state nonlinear vibration isolator with symmetric permanent magnets," *Nonlinear Dynamics*, vol. 97, no. 4, pp. 2499–2519, 2019.

[13] Q. Zhang, S. Xia, D. Xu, and Z. Peng, "A torsion-translational vibration isolator with quasi-zero stiffness," *Nonlinear Dynamics*, vol. 99, no. 2, pp. 1467–1488, 2020.

[14] K. Wang, J. Zhou, Y. Chang, H. Ouyang, D. Xu, and Y. Yang, "A nonlinear ultra-low-frequency vibration isolator with dual quasi-zero-stiffness mechanism," *Nonlinear Dynamics*, vol. 101, no. 2, pp. 755–773, 2020.

[15] K. Watanabe and S. Nakai, "Vibration control of strongly nonlinear stiffness device combined with large virtual mass," *Journal of Structural and Construction Engineering (Transactions of AIJ)*, vol. 81, no. 722, pp. 675–683, 2016.

[16] Y. Zhou, P. Chen, and G. Mosqueda, "Analytical and numerical investigation of quasi-zero stiffness vertical isolation system," *Journal of Engineering Mechanics*, vol. 145, no. 6, Article ID 04019035, 2019.

[17] D. Liu, Y. Liu, D. Sheng, and W. Liao, "Seismic response analysis of an isolated structure with QZS under near-fault vertical earthquakes," *Shock and Vibration*, vol. 2018, Article ID 9149721, pp. 1–12, 2018.

[18] H. Li, Y. Li, and J. Li, "Negative stiffness devices for vibration isolation applications: a review," *Advances in Structural Engineering*, vol. 23, no. 8, pp. 1739–1755, 2020.

[19] J. Yang, J. Z. Jiang, and S. A. Neild, "Dynamic analysis and performance evaluation of nonlinear inerter-based vibration isolators," *Nonlinear Dynamics*, vol. 99, no. 3, pp. 1823–1839, 2020.

[20] A. Carrella, *Passive Vibration Isolators with High-Static-Low-Dynamic-Stiffness-Basic Principles and Design of HSLDS Mechanisms*, VDM Verlag Dr. Mueller, Saarbrücken, Germany, 2010.

[21] FEMA, "P695 quantification of building seismic performance factors," 2009, https://www.fema.gov/media-library-data/20130726-1716-25045-9655/fema%20p695.pdf.

[22] K. Miyamoto, J. Iba, K. Watanabe, K. Ishii, and M. Kikuchi, "Experimental verication of analysis model of seismic isolation with high-static-low-dynamic stiffness," pp. 1–26, 2021, https://www.researchsquare.com/article/rs-1102839/v1.

[23] A. Carrella, M. J. Brennan, and T. P. Waters, "Static analysis of a passive vibration isolator with quasi-zero-stiffness characteristic," *Journal of Sound and Vibration*, vol. 301, no. 3-5, pp. 678–689, 2007.